TABLE 1 PV antigens in RIG-I- and MDA5-deficient mice

| Organ or tissue | No. of PV antigen-positive mice/no. of mice tested | | | |
|---|---|---|---|---|
| | RIG-I$^{+/-}$ MDA5$^{+/-}$ | RIG-I$^{-/-}$ MDA5$^{+/-}$ | RIG-I$^{+/-}$ MDA5$^{-/-}$ | RIG-I$^{-/-}$ MDA5$^{-/-}$ |
| Brain | 4/4 | 3/3 | 4/4 | 4/4 |
| Spinal cord | 4/4 | 3/3 | 4/4 | 4/4 |
| Heart | 0/4 | 0/3 | 0/4 | 0/4 |
| Lung | 0/4 | 0/3 | 0/4 | 0/4 |
| Liver | 0/4 | 0/3 | 0/4 | 0/4 |
| Kidney | 0/4 | 0/3 | 0/4 | 0/4 |
| Spleen | 0/4 | 0/3 | 0/4 | 0/4 |
| Pancreas | 0/4 | 0/3 | 0/4 | 0/4 |
| Intestine | 0/4 | 0/3 | 0/4 | 0/4 |
| Adipose tissue | 0/4 | 0/3 | 0/4 | 0/4 |

mice in the ICR background after intravenous infection with PV at $10^3$, $10^4$, and $10^5$ PFU (Fig. 5A, B, and C). The mortality rates of these mice did not differ significantly from each other. We observed that the mortality rates of RIG-I$^{+/-}$ MDA5$^{-/-}$ mice that were inoculated with $10^4$ PFU of PV was slightly higher than the mice of other genotypes. However, significant differences were not observed in mice that were inoculated with the other doses. Similar experiments were performed using MDA5$^{-/-}$ and MDA5$^{+/-}$ mice in the B6 background (Fig. 5D, E, and F). We did not observe significant differences between the MDA5$^{-/-}$ and MDA5$^{+/-}$ mice. The mortality rate of MDA5$^{-/-}$ mice was slightly higher than that of MDA5$^{+/-}$ mice that were inoculated with $10^5$ PFU of PV. However, the opposite trend was observed when mice

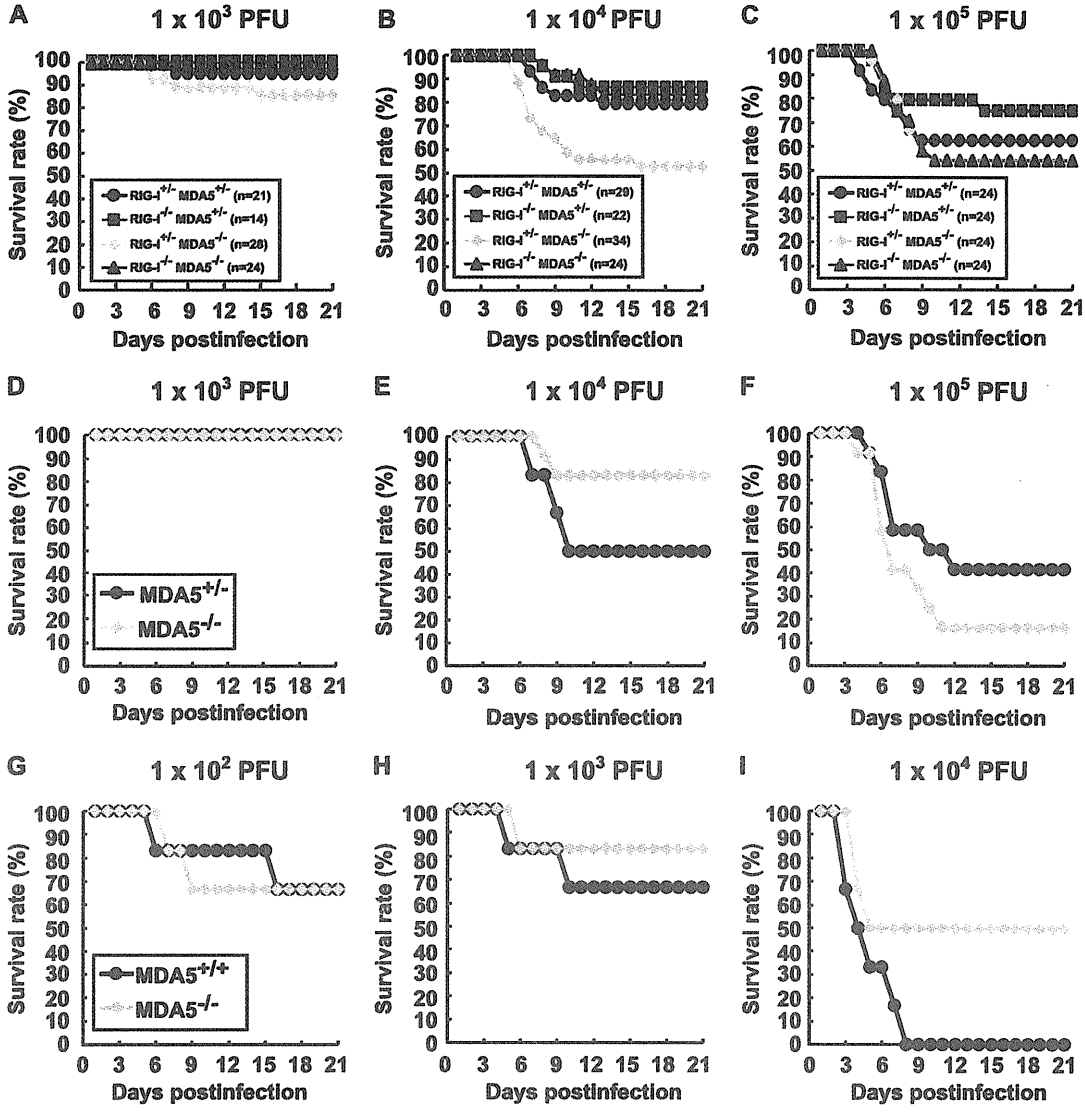


FIG 5 Mortality rates of RIG-I- and MDA5-deficient mice. Littermates of the genotypes indicated were obtained by mating RIGI-I$^{+/-}$ MDA5$^{+/-}$ and RIGI-I$^{-/-}$ MDA5$^{-/-}$ mice in the ICR background. The mice were infected intravenously with $10^3$ (A), $10^4$ (B), or $10^5$ (C) PFU of PV. The results shown are the sums of several independent experiments. The total numbers of mice of the different genotypes that were used are boxed, and the doses used are shown at the top. Littermates of MDA5$^{+/-}$ and MDA5$^{-/-}$ mice were obtained in the B6 background. The mice ($n$ = 12) were intravenously infected with $10^3$ (D), $10^4$ (E), or $10^5$ (F) of PV. MDA5$^{+/+}$ and MDA5$^{-/-}$ mice ($n$ = 6) were intracerebrally infected with $10^2$ (G), $10^3$ (H), or $10^4$ (I) PFU of PV, respectively. We monitored the survival rates of the mice for 3 weeks after infection.

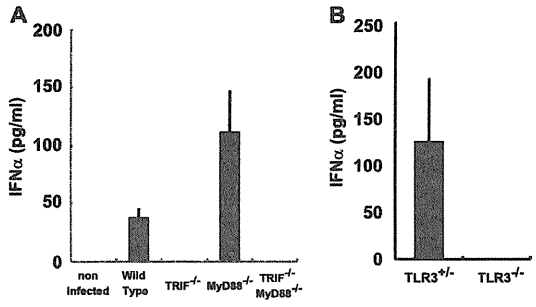


FIG 6 Production of serum IFN-$\alpha$ in TRIF-, MyD88-, and TLR3-deficient mice. Mice ($n$ = 3 or 8) were intravenously infected with $10^7$ PFU of PV. IFN-$\alpha$ levels of TRIF- and MyD88-deficient mice (A) and TLR3-deficient mice (B) at 12 hpi were compared. The experiments were repeated twice, and representative data are shown.

were inoculated with $10^4$ PFU of PV. We suspect that the slight difference between the mortality rates of wild-type and MDA5$^{-/-}$ mice was in the range of experimental fluctuation, and thus, the disruption of MDA5 did not significantly influence the mortality rate. In order to determine if the same is true when mice are infected by other routes, we inoculated wild-type and MDA5$^{-/-}$ mice with PV intracerebrally and compared their mortality rates (Fig. 5G to I). Their mortality rates did not differ significantly. These results suggest that MDA5 does not make a great contribution to the protection of mice, at least after intracerebral and intravenous infections. Taken together, the MDA5-mediated response does not play a dominant role in IFN production, ISG induction, or inhibition of PV replication *in vivo*, unlike the MDA5-mediated effects on EMCV infection.

**IFN response in TRIF- and MyD88-deficient mice.** Because the experiments with MDA5-deficient mice suggested the existence of other protective mechanisms in PV infection, we investigated the role of TLRs using TRIF- and MyD88-deficient mice. PVR-tg mice were mated with TRIF$^{-/-}$ and/or MyD88$^{-/-}$ mice in the B6 background. Serum IFN-$\alpha$ of mice infected with $10^7$ PFU of PV was measured using ELISA at 12 hpi (Fig. 6A). Interestingly, serum IFN production in response to PV infection was abrogated in TRIF$^{-/-}$ mice. Because TRIF acts as an adaptor for TLR3 and TLR4, we tested whether the same phenomenon occurs in TLR3$^{-/-}$ mice. Serum IFN induction was not observed in TLR3-deficient mice (Fig. 6B). These results suggest that the TLR3-mediated pathway is essential for IFN production in response to PV infection.

We next assessed the induction of mRNAs for OAS1a (Fig. 7A) and IRF-7 (Fig. 7B) in various organs using real-time RT-PCR. The induction of OAS1a and IRF-7 was observed in all mice. Although serum IFN production was abrogated in TRIF$^{-/-}$ mice and TRIF$^{-/-}$ MyD88$^{-/-}$ mice (Fig. 6), a significant level of ISG mRNA was induced. However, the induction levels were slightly lower than those in wild-type mice in some cases. The results suggest that the TRIF-mediated pathway contributes to ISG expression mainly through the induction of serum IFNs in response to PV infection and that some other mechanisms may also contribute to ISG expression.

**PV replication in nonneural tissues and mortality rates of TRIF- and MyD88-deficient mice.** The brain, spinal cord, liver, spleen, and kidney of paralyzed mice were recovered, and viral titers were determined (Fig. 8). PV was recovered from the CNS of TRIF$^{-/-}$, MyD88$^{-/-}$, and TLR3$^{-/-}$ mice, and the titers were not different from those of wild-type mice. However, the viral titers of the liver, spleen, and kidney of TRIF$^{-/-}$ and TLR3$^{-/-}$ mice were significantly higher than those of wild-type mice but lower than those of IFNAR1$^{-/-}$ mice. We then examined the virus replication kinetics in TRIF$^{-/-}$ mice (Fig. 8B). The viral load in the CNS increased in TRIF$^{-/-}$ mice similarly to that in other mice. In accordance to the absence of serum IFN (Fig. 2), the viral loads in the liver, spleen, and kidney of TRIF$^{-/-}$ mice increased, while the viral loads in these organs of wild-type mice decreased. PV antigens were detected in the CNS of all of the knockout mice. In addition, PV antigens were detected in the adipose tissue, pancreas, and kidney of several TRIF$^{-/-}$ and MyD88$^{-/-}$ mice (Table 2). These results suggest that these tissues support viral multiplication in these knockout mice and that the TLR-mediated signaling pathways contribute to the regulation of PV replication in nonneural tissues.

The mortality rates of TRIF$^{-/-}$, MyD88$^{-/-}$, and TLR3$^{-/-}$

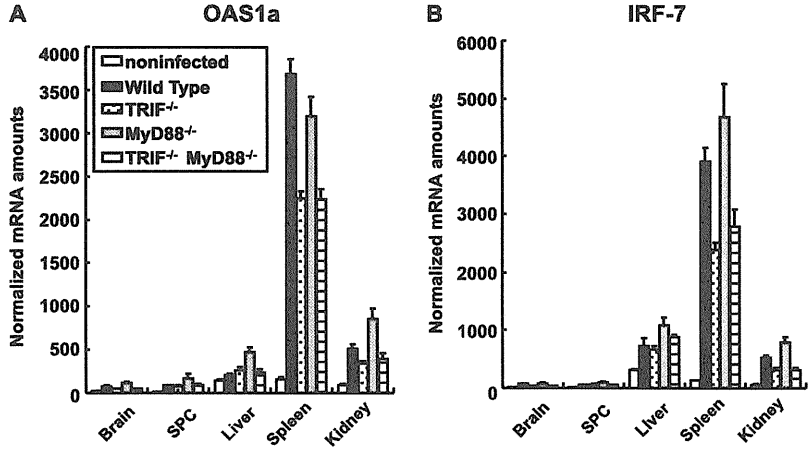


FIG 7 ISG induction in TRIF- and MyD88-deficient mice. Mice ($n$ = 4) were intravenously infected with $10^7$ PFU of PV. At 12 hpi, RNA was isolated from the indicated tissues of the infected mice and OAS1a (A) and IRF-7 (B) mRNA levels were determined by quantitative real-time PCR. The experiments were repeated twice, and representative data are shown. SPC, spinal cord.

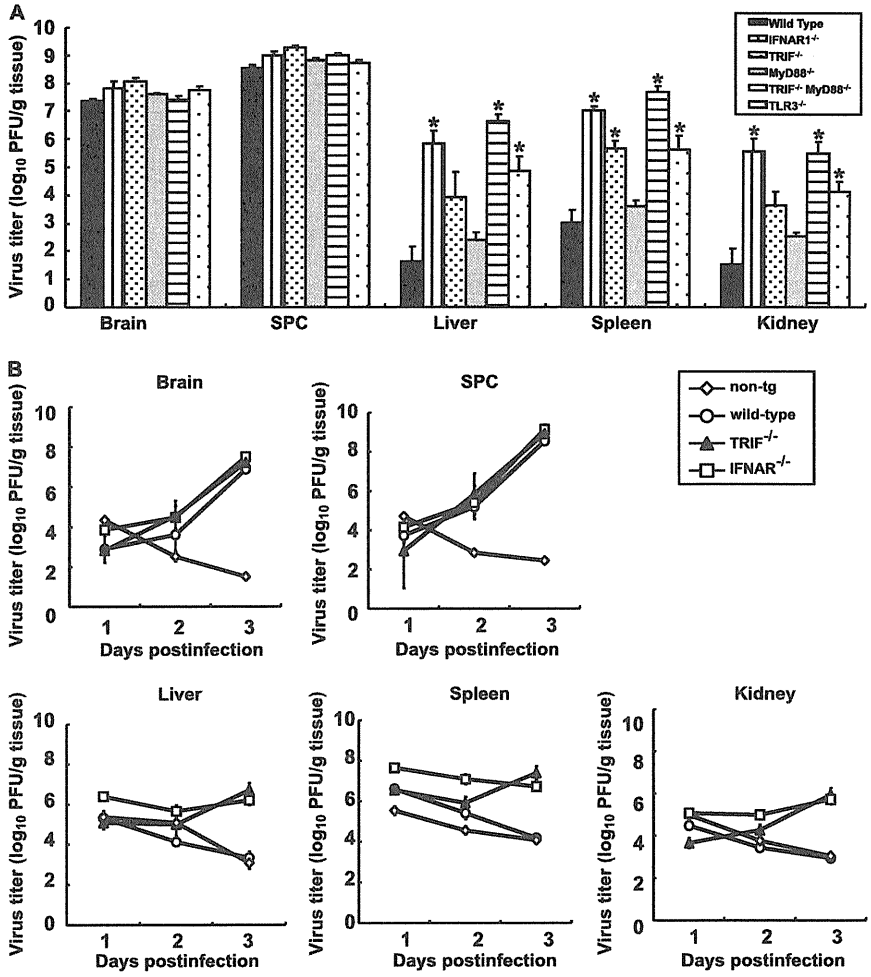


FIG 8 (A) PV replication in TRIF- and MyD88-deficient mice. Wild-type ($n = 4$), TRIF$^{-/-}$ ($n = 4$), MyD88$^{-/-}$ ($n = 6$), TRIF$^{-/-}$ MyD88$^{-/-}$ ($n = 4$), TLR3$^{-/-}$ ($n = 5$), and IFNAR1$^{-/-}$ ($n = 4$) mice were intravenously infected with $10^7$ PFU of PV. The infected mice were paralyzed or dead at 3 to 5 days postinfection. The indicated tissues were collected, and viral titers were determined using a plaque assay (*, $P < 0.01$ by $t$ test compared to wild-type mice). (B) PV replication kinetics in TRIF-deficient mice. Nontransgenic mice, wild-type mice, TRIF$^{-/-}$ mice, and IFNAR1$^{-/-}$ mice ($n = 3$) were infected as described above. Tissues were collected daily, and viral titers were determined. The results for nontransgenic (non-tg) mice, wild-type mice, and IFNAR1$^{-/-}$ mice are the same as those in Fig. 4B. SPC, spinal cord.

TABLE 2 PV antigens in TRIF- and MyD88-deficient mice

| Organ or tissue | No. of PV antigen-positive mice/no. of mice tested | | | |
|---|---|---|---|---|
| | Wild type | TRIF$^{-/-}$ | MyD88$^{-/-}$ | TRIF$^{-/-}$ MyD88$^{-/-}$ |
| Brain | 6/6 | 8/8 | 9/9 | 6/6 |
| Spinal cord | 6/6 | 8/8 | 9/9 | 6/6 |
| Heart | 0/6 | 0/8 | 0/8 | 0/6 |
| Lung | 0/6 | 0/8 | 0/8 | 0/6 |
| Liver | 0/6 | 0/8 | 0/9 | 0/6 |
| Kidney | 0/6 | 0/8 | 2/9 | 0/5 |
| Spleen | 0/6 | 0/8 | 0/9 | 0/6 |
| Pancreas | 2/6 | 0/8 | 7/9 | 4/6 |
| Intestine | 0/6 | 0/8 | 0/9 | 0/6 |
| Adipose tissue | 0/6 | 2/8 | 2/9 | 3/6 |

mice were compared (Fig. 9). Approximately 25% of the TRIF$^{-/-}$ mice died after infection with $10^2$ PFU of PV, and almost all of the mice died after infection with more than $10^3$ PFU of PV (Fig. 9A). Approximately 20% and 60% of the MyD88$^{-/-}$ mice died after infection with $10^3$ and $10^4$ PFU of PV, respectively (Fig. 9B and C). TRIF$^{-/-}$ MyD88$^{-/-}$ mice were the most susceptible. In total, 70% of the mice died after infection with $10^2$ PFU of PV (Fig. 9A). The mortality rate of TRIF$^{-/-}$ MyD88$^{-/-}$ mice was very close to that of IFNAR1$^{-/-}$ mice (19). The mortality rate of TLR3$^{-/-}$ mice was similar to that of TRIF$^{-/-}$ mice (Fig. 9D, E, and F). These results suggest that the TRIF-mediated and MyD88-mediated antiviral responses contribute to the host's defense against PV infection and that the TLR3-TRIF-mediated response has the most dominant effect.

## DISCUSSION

Each virus infects different cell types and has a characteristic mode of replication. In mammalian hosts, several viral RNA sensors,

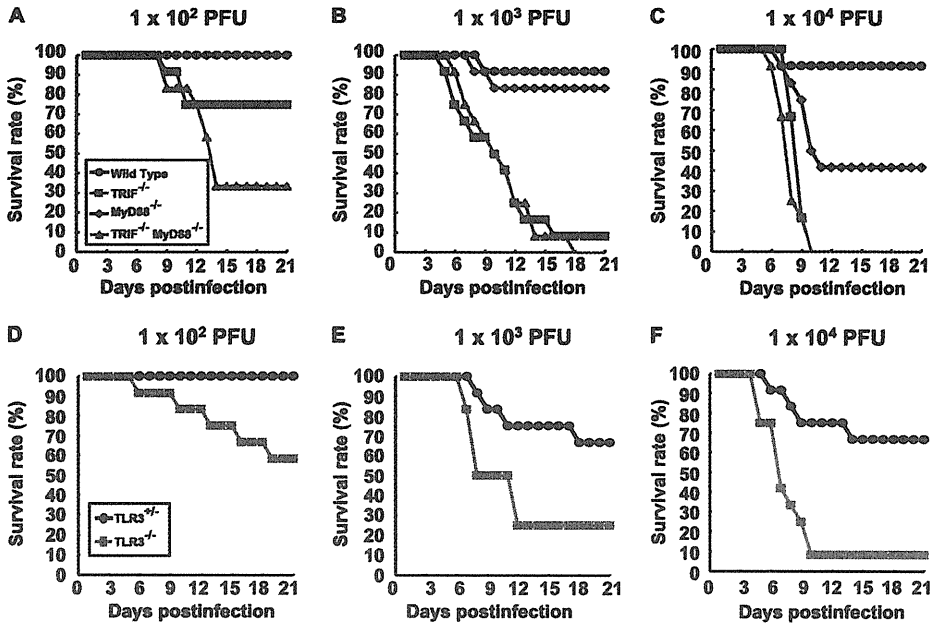


FIG 9 Mortality rates of TRIF-, MyD88-, and TLR3-deficient mice. (A) Wild-type, TRIF$^{-/-}$, MyD88$^{-/-}$, and TRIF$^{-/-}$ MyD88$^{-/-}$ mice ($n$ = 12) were intravenously inoculated with the indicated doses of PV. (B) Littermates of TLR3$^{+/-}$ and TLR3$^{-/-}$ mice ($n$ = 12) were used.

which are expressed in different cell types and recognize different molecular patterns, have evolved to counteract a variety of viruses. In the present study, we demonstrated that the MDA5-, TRIF-, and MyD88-mediated pathways contribute to the recognition of PV infection and that the TLR3-TRIF-mediated pathway plays the most important role in the antiviral response. Since all of the phenotypes shown after PV infection in the TRIF$^{-/-}$ mice and TLR3$^{-/-}$ mice are very similar to each other, we think that the contribution of the TLR3-mediated response is dominant and that of the TLR4-mediated response is negligible.

Previous reports have revealed that IFN is produced efficiently in EMCV-infected fibroblasts in an MDA5-dependent manner and that MDA5 contributes to the induction of serum IFNs and the protection of mice against EMCV (10, 23). Because EMCV belongs to the family *Picornaviridae*, we hypothesized that MDA5 also contributes to IFN induction in response to PV infection. However, the MDA5-dependent pathway did not play a dominant role in the defense against PV infection. Therefore, we speculate that PV uses mechanisms different from those of EMCV to strongly suppress IFN production *in vivo*. Indeed, IFN production in cultured cells in response to PV infection was observed only when the cells were pretreated with a low dose of IFNs. In addition, the amount of IFN produced was much lower than that produced in response to EMCV infection (Fig. 1). This result suggests that IFN induction in infected cells is suppressed and that this PV-mediated effect may be stronger than that of EMCV. Translational shutoff may be one of the reasons for this difference. PV 3A protein causes a change in membrane trafficking that prevents protein secretion and may also contribute to the suppression of IFN production (6). Caspase-dependent cleavage of MDA5 (3) and IPS-1 (39) in PV-infected cells has been reported. Through these possible mechanisms, PV may induce the suppression of IFN production in mice *in vivo*, and the MDA5-mediated pathway does not play an essential role in the host response, unlike in EMCV infection. PV and EMCV seemed to use different strategies to counteract the host innate immune system, even though PV and EMCV belong to the same family. Thus, TLR3 became the sensor that functions most effectively for PV as a result of PV evolution. Although the TLR3-TRIF-mediated pathway plays a dominant role, the fact that significant ISG induction was observed in PV-infected TRIF$^{-/-}$ and TRIF$^{-/-}$ MyD88$^{-/-}$ mice (Fig. 7) suggested that other mechanisms also operate in combination with this pathway.

The viral loads in the nonneural tissues of TLR3- and TRIF-deficient mice were much higher than those in wild-type mice, whereas the viral loads in the CNS were not significantly different in paralyzed mice (Fig. 8). These results suggest that the TLR3-TRIF-mediated pathway inhibits viral replication mainly before viral invasion of the CNS rather than after invasion and that this response plays an important role in preventing the viral invasion of the CNS. In the CNS, replication of PV was not effectively inhibited, even in wild-type mice. This result is consistent with our previous results obtained using IFNAR1$^{-/-}$ mice and suggests that the antivirus response in the CNS is different from that in nonneural tissues upon PV infection (19). The cell tropism of PV may influence the efficiency of the immune response. For example, if PVR is expressed in TLR3-expressing cells, then PV replication would be detected immediately after infection. Alternatively, if PV infection *in vivo* occurs in the vicinity of TLR3-expressing immune cells such as DCs and macrophages, PV-infected cells may readily be captured by TLR3-expressing cells, thereby facilitating efficient cross-priming (27, 44) of PV RNA. PV infects neurons almost exclusively and not other cell types in the CNS. If neurons do not have the ability to induce a strong TLR3-mediated antiviral response upon PV infection, the CNS may be more defective in the innate immune response than nonneural tissues are. This may be one of the reasons why PV replicates preferentially in the CNS. Further studies on PV pathogenesis related to the innate

immune response will make a great contribution to elucidating the mechanisms of PV tissue tropism.

TLR3 recognizes dsRNA. However, the protective role of TLR3 in the response to many RNA viral infections is not clear (9, 29, 43). A previous study has demonstrated that WNV, which is an encephalitis virus belonging to the family *Flaviviridae*, causes more severe encephalitis in mice with intact TLR3 than in TLR3$^{-/-}$ mice. Peripheral WNV infection leads to a breakdown of the blood-brain barrier (BBB) and enhances brain infection in wild-type mice but not in TLR3$^{-/-}$ mice (50). In contrast, a protective role of the TLR3-mediated pathway in PV infection was clearly demonstrated in the present study. PV enters the CNS directly across the BBB via a PVR-independent mechanism (52) and from the neuromuscular junction via retrograde axonal transport (31–33). Because PV originally possesses two entry pathways into the CNS, the generation of a new entry pathway, even if it did occur, might not increase its deteriorative effect.

Interestingly, protective roles of the TLR3-mediated pathway have been reported for group B coxsackievirus (30, 41, 42), human rhinovirus (49), and EMCV (11) infections. Riad et al. (41) demonstrated that TRIF$^{-/-}$ mice showed severe myocarditis after CVB3 infection and IFN-$\beta$ treatment improved virus control and reduced cardiac inflammation. Richer et al. (42) reported that TLR3$^{-/-}$ mice produced reduced proinflammatory mediators and were unable to control CVB4 replication at the early stages of infection, resulting in severe cardiac damage. They also showed that adoptive transfer of wild-type macrophages into TLR3$^{-/-}$ mice challenged with CVB4 resulted in greater survival, suggesting the importance of the TLR3-mediated pathway in the macrophage. Negishi et al. (30) reported that TLR3$^{-/-}$ mice showed vulnerability to CVB3 and that TLR3 signaling is linked to the activation of the type II IFN system. Since CVB3 does not induce robust type I IFNs, they suggested that the TLR3 type II IFN pathway serves as an "ace in the hole" in infections with such viruses. PV is similar to CVB3 because type I IFN production is low. However, in our preliminary experiments on PV infection in IFN-$\gamma^{-/-}$ PVR-tg mice, type II IFN did not make a significant contribution to the pathogenesis of PV. Taken together, these results suggest a critical role for the TLR3-mediated pathway, but the precise mechanisms leading to host protection are still controversial and the downstream events of TLR3 signaling after picornavirus infection remain to be elucidated.

Because the above-mentioned viruses are picornaviruses, picornavirus RNA may be easily detected by TLR3. There may be a common RNA structure in the genome or in the replication intermediates of these viruses that is detected by TLR3. Alternatively, picornaviral RNA may replicate in a compartment in which TLR3 can easily access the replicating dsRNA. To investigate these hypotheses, identification of the cells responsible for IFN production is an important step. Oshiumi et al. demonstrated that splenic CD8$\alpha^+$ CD11c$^+$ cells, bone marrow-derived macrophages, and DCs are able to elicit IFN in response to PV infection (35). Further studies using this virus-cell system will elucidate the molecular recognition pattern in the PV genome, the precise mechanism of PV RNA recognition in TLR3-expressing cells, and the roles of these cells in the prevention of PV dissemination in the body.

## ACKNOWLEDGMENTS

We thank Takashi Fujita, Mitsutoshi Yoneyama, Hiroki Kato, Masahiro Yamamoto, Satoshi Uematsu, Seiya Yamayoshi, Akira Ainai, Hideki Hasegawa, and Takashi Kawanishi for helpful discussions and technical assistance.

This work was supported, in part, by Grants-in-Aid from the Ministry of Education, Culture, Sports, Science and Technology, Japan (Grants-in-Aid for Scientific Research on Priority Areas no. 21022053), and Grants-in-Aid for Research on Emerging and Re-emerging Infectious Diseases from the Ministry of Health, Labor and Welfare, Japan.

## REFERENCES

1. **Akira S, Uematsu S, Takeuchi O.** 2006. Pathogen recognition and innate immunity. Cell **124**:783–801.
2. **Alexopoulou L, Holt AC, Medzhitov R, Flavell RA.** 2001. Recognition of double-stranded RNA and activation of NF-kappaB by Toll-like receptor 3. Nature **413**:732–738.
3. **Barral PM, et al.** 2007. MDA-5 is cleaved in poliovirus-infected cells. J. Virol. **81**:3677–3684.
4. **Bodian D.** 1959. Poliomyelitis: pathogenesis and histopathology, p 479–518. *In*Rivers TM, Horsfall FL, Jr (ed), Viral and rickettsial infections of man, vol 3. J. B. Lippincott, Philadelphia, PA.
5. **Cella M, et al.** 1999. Plasmacytoid monocytes migrate to inflamed lymph nodes and produce large amounts of type I interferon. Nat. Med. **5**:919–923.
6. **Choe SS, Dodd DA, Kirkegaard K.** 2005. Inhibition of cellular protein secretion by picornaviral 3A proteins. Virology **337**:18–29.
7. **Colonna M, Trinchieri G, Liu YJ.** 2004. Plasmacytoid dendritic cells in immunity. Nat. Immunol. **5**:1219–1226.
8. **Diebold SS, Kaisho T, Hemmi H, Akira S, Reis e Sousa C.** 2004. Innate antiviral responses by means of TLR7-mediated recognition of single-stranded RNA. Science **303**:1529–1531.
9. **Edelmann KH, et al.** 2004. Does Toll-like receptor 3 play a biological role in virus infections? Virology **322**:231–238.
10. **Gitlin L, et al.** 2006. Essential role of mda-5 in type I IFN responses to polyriboinosinic:polyribocytidylic acid and encephalomyocarditis picornavirus. Proc. Natl. Acad. Sci. U. S. A. **103**:8459–8464.
11. **Hardarson HS, et al.** 2007. Toll-like receptor 3 is an essential component of the innate stress response in virus-induced cardiac injury. Am. J. Physiol. Heart Circ. Physiol. **292**:H251–H258.
12. **Hemmi H, et al.** 2002. Small anti-viral compounds activate immune cells via the TLR7 MyD88-dependent signaling pathway. Nat. Immunol. **3**:196–200.
13. **Hoebe K, et al.** 2003. Identification of Lps2 as a key transducer of MyD88-independent TIR signalling. Nature **424**:743–748.
14. **Holland JJ.** 1961. Receptor affinities as major determinants of enterovirus tissue tropisms in humans. Virology **15**:312–326.
15. **Holland JJ, Mc LL, Syverton JT.** 1959. Mammalian cell-virus relationship. III. Poliovirus production by non-primate cells exposed to poliovirus ribonucleic acid. Proc. Soc. Exp. Biol. Med. **100**:843–845.
16. **Holland JJ, McLaren LC, Syverton JT.** 1959. The mammalian cell-virus relationship. IV. Infection of naturally insusceptible cells with enterovirus ribonucleic acid. J. Exp. Med. **110**:65–80.
17. **Hornung V, et al.** 2006. 5′-Triphosphate RNA is the ligand for RIG-I. Science **314**:994–997.
18. **Hsiung GD, Black FL, Henderson JR.** 1964. Susceptibility of primates to viruses in relation to taxonomic classification, p 1–23. *In*Buettner-Jaenusch J (ed), Evolutionary and genetic biology of primates, vol 2. Academic Press, New York, NY.
19. **Ida-Hosonuma M, et al.** 2005. The alpha/beta interferon response controls tissue tropism and pathogenicity of poliovirus. J. Virol. **79**: 4460–4469.
20. **Ida-Hosonuma M, et al.** 2003. Host range of poliovirus is restricted to simians because of a rapid sequence change of the poliovirus receptor gene during evolution. Arch. Virol. **148**:29–44.
21. **Kato H, et al.** 2005. Cell type-specific involvement of RIG-I in antiviral response. Immunity **23**:19–28.
22. **Kato H, et al.** 2008. Length-dependent recognition of double-stranded ribonucleic acids by retinoic acid-inducible gene-I and melanoma differentiation-associated gene 5. J. Exp. Med. **205**:1601–1610.
23. **Kato H, et al.** 2006. Differential roles of MDA5 and RIG-I helicases in the recognition of RNA viruses. Nature **441**:101–105.
24. **Koike S, et al.** 1992. A second gene for the African green monkey poliovirus receptor that has no putative N-glycosylation site in the functional N-terminal immunoglobulin-like domain. J. Virol. **66**:7059–7066.

25. **Koike S, Nomoto A.** 2010. Poliomyelitis, p 339–351. *In*Ehrenfeld E, Domingo E, Roos RP (ed), The picornaviruses. ASM Press, Washington, DC.
26. **Koike S, et al.** 1991. Transgenic mice susceptible to poliovirus. Proc. Natl. Acad. Sci. U. S. A. **88**:951–955.
27. **Kramer M, et al.** 2008. Phagocytosis of picornavirus-infected cells induces an RNA-dependent antiviral state in human dendritic cells. J. Virol. **82**:2930–2937.
28. **Matsumoto M, et al.** 2003. Subcellular localization of Toll-like receptor 3 in human dendritic cells. J. Immunol. **171**:3154–3162.
29. **Matsumoto M, Oshiumi H, Seya T.** 2011. Antiviral responses induced by the TLR3 pathway. Rev. Med. Virol. **21**:67–77.
30. **Negishi H, et al.** 2008. A critical link between Toll-like receptor 3 and type II interferon signaling pathways in antiviral innate immunity. Proc. Natl. Acad. Sci. U. S. A. **105**:20446–20451.
31. **Ohka S, et al.** 2004. Receptor (CD155)-dependent endocytosis of poliovirus and retrograde axonal transport of the endosome. J. Virol. **78**: 7186–7198.
32. **Ohka S, et al.** 2009. Receptor-dependent and -independent axonal retrograde transport of poliovirus in motor neurons. J. Virol. **83**:4995–5004.
33. **Ohka S, Yang WX, Terada E, Iwasaki K, Nomoto A.** 1998. Retrograde transport of intact poliovirus through the axon via the fast transport system. Virology **250**:67–75.
34. **Oshiumi H, Matsumoto M, Funami K, Akazawa T, Seya T.** 2003. TICAM-1, an adaptor molecule that participates in Toll-like receptor 3-mediated interferon-beta induction. Nat. Immunol. **4**:161–167.
35. **Oshiumi H, et al.** 12 October 2011, posting date. The TLR3-TICAM-1 pathway is mandatory for innate immune responses to poliovirus infection. J. Immunol. [Epub ahead of print.] doi:10.4049/jimmunol.1101503.
36. **Pichlmair A, et al.** 2006. RIG-I-mediated antiviral responses to single-stranded RNA bearing 5′-phosphates. Science **314**:997–1001.
37. **Pichlmair A, et al.** 2009. Activation of MDA5 requires higher-order RNA structures generated during virus infection. J. Virol. **83**:10761–10769.
38. **Racaniello VR.** 2007. Picornaviridae: the viruses and their replication, p 795–838. *In*Knipe DM, Howley PM (ed), Fields virology, 5th ed. Lippincott Williams & Wilkins, Philadelphia, PA.
39. **Rebsamen M, Meylan E, Curran J, Tschopp J.** 2008. The antiviral adaptor proteins Cardif and Trif are processed and inactivated by caspases. Cell Death Differ. **15**:1804–1811.
40. **Ren RB, Costantini F, Gorgacz EJ, Lee JJ, Racaniello VR.** 1990. Transgenic mice expressing a human poliovirus receptor: a new model for poliomyelitis. Cell **63**:353–362.
41. **Riad A, et al.** 2011. TRIF is a critical survival factor in viral cardiomyopathy. J. Immunol. **186**:2561–2570.
42. **Richer MJ, Lavallee DJ, Shanina I, Horwitz MS.** 2009. Toll-like receptor 3 signaling on macrophages is required for survival following coxsackievirus B4 infection. PLoS One **4**:e4127.
43. **Schröder M, Bowie AG.** 2005. TLR3 in antiviral immunity: key player or bystander? Trends Immunol. **26**:462–468.
44. **Schulz O, et al.** 2005. Toll-like receptor 3 promotes cross-priming to virus-infected cells. Nature **433**:887–892.
45. **Shiroki K, et al.** 1995. A new *cis*-acting element for RNA replication within the 5′ noncoding region of poliovirus type 1 RNA. J. Virol. **69**: 6825–6832.
46. **Takeuchi O, Akira S.** 2009. Innate immunity to virus infection. Immunol. Rev. **227**:75–86.
47. **Takeuchi O, Akira S.** 2008. MDA5/RIG-I and virus recognition. Curr. Opin. Immunol. **20**:17–22.
48. **Takeuchi O, Akira S.** 2007. Recognition of viruses by innate immunity. Immunol. Rev. **220**:214–224.
49. **Wang Q, et al.** 2009. Role of double-stranded RNA pattern recognition receptors in rhinovirus-induced airway epithelial cell responses. J. Immunol. **183**:6989–6997.
50. **Wang T, et al.** 2004. Toll-like receptor 3 mediates West Nile virus entry into the brain causing lethal encephalitis. Nat. Med. **10**:1366–1373.
51. **Yamamoto M, et al.** 2003. Role of adaptor TRIF in the MyD88-independent Toll-like receptor signaling pathway. Science **301**:640–643.
52. **Yang WX, et al.** 1997. Efficient delivery of circulating poliovirus to the central nervous system independently of poliovirus receptor. Virology **229**:421–428.
53. **Yoneyama M, et al.** 2004. The RNA helicase RIG-I has an essential function in double-stranded RNA-induced innate antiviral responses. Nat. Immunol. **5**:730–737.
54. **Yoshikawa T, et al.** 2006. Role of the alpha/beta interferon response in the acquisition of susceptibility to poliovirus by kidney cells in culture. J. Virol. **80**:4313–4325.
55. **Yousefi S, Escobar MR, Gouldin CW.** 1985. A practical cytopathic effect/dye-uptake interferon assay for routine use in the clinical laboratory. Am. J. Clin. Pathol. **83**:735–740.

OPEN ACCESS Freely available online

PLoS one

# UNC93B1 Physically Associates with Human TLR8 and Regulates TLR8-Mediated Signaling

**Hiroki Itoh[☯], Megumi Tatematsu[☯], Ayako Watanabe[☯¤], Katsunori Iwano, Kenji Funami, Tsukasa Seya, Misako Matsumoto***

Department of Microbiology and Immunology, Hokkaido University Graduate School of Medicine, Sapporo, Japan

## Abstract

Toll-like receptors (TLRs) 3, 7, 8, and 9 are localized to intracellular compartments where they encounter foreign or self nucleic acids and activate innate and adaptive immune responses. The endoplasmic reticulum (ER)-resident membrane protein, UNC93B1, is essential for intracellular trafficking and endolysosomal targeting of TLR7 and TLR9. TLR8 is phylogenetically and structurally related to TLR7 and TLR9, but little is known about its localization or function. In this study, we demonstrate that TLR8 localized to the early endosome and the ER but not to the late endosome or lysosome in human monocytes and HeLa transfectants. UNC93B1 physically associated with human TLR8, similar to TLRs 3, 7, and 9, and played a critical role in TLR8-mediated signaling. Localization analyses of TLR8 tail-truncated mutants revealed that the transmembrane domain and the Toll/interleukin-1 receptor domain were required for proper targeting of TLR8 to the early endosome. Hence, although UNC93B1 participates in intracellular trafficking and signaling for all nucleotide-sensing TLRs, the mode of regulation of TLR localization differs for each TLR.

**Citation:** Itoh H, Tatematsu M, Watanabe A, Iwano K, Funami K, et al. (2011) UNC93B1 Physically Associates with Human TLR8 and Regulates TLR8-Mediated Signaling. PLoS ONE 6(12): e28500. doi:10.1371/journal.pone.0028500

**Editor:** Nick Gay, University of Cambridge, United Kingdom

**Received** August 3, 2011; **Accepted** November 9, 2011; **Published** December 2, 2011



**Funding:** This work was supported in part by Grants-in-Aid from the Ministry of Education, Science, and Culture, the Ministry of Health, Labor, and Welfare of Japan, and by the Akiyama Life Science Foundation. The funders had no role in study design, data collection and analysis, decision to publish, or preparation of the manuscript.

**Competing Interests:** The authors have declared that no competing interests exist.

* E-mail: matumoto@pop.med.hokudai.ac.jp

☯ These authors contributed equally to this work.

¤ Current address: Department of Cancer Biology, The Institute of Medical Science, The University of Tokyo, Tokyo, Japan

## Introduction

The innate immune system discriminates self from non-self by expressing germ-line encoded receptors that recognize pathogen- or damage-associated molecular patterns [1-3]. The Toll-like receptor (TLR) family of type I transmembrane proteins were the first group of pattern recognition receptors to be identified [4]. Within this family, TLRs 3, 7, 8, and 9 recognize microbial nucleic acids and induce cytokine production, including type I interferon (IFN), and dendritic cell (DC) maturation [2]. In humans, TLR7 and TLR9 are selectively expressed in B cells and plasmacytoid DCs, while TLR3 and TLR8 are expressed in myeloid DCs [5–8].

TLR8 is phylogenetically and structurally related to TLR7 [9,10]; they both recognize ssRNA and an imidazoquinoline compound [11–13]. In mice, TLR8 appears to be nonfunctional in most tissues and cells, except for the brain [14,15]. Human TLR8 is expressed in myeloid cells, such as monocytes, macrophages, and myeloid DCs, and also, in regulatory T cells [6,16,17]. Upon stimulation with synthetic ligands, human TLR8 activates NF-κB via the adaptor protein MyD88, which leads to the induction of proinflammatory cytokines but, not type I IFN [13]. In contrast, human/mouse TLR7 strongly induces type I IFN production in response to ssRNA and an imidazoquinoline compound. The differential expression and cytokine profiles of human TLR8 compared with those of human/mouse TLR7 suggest that human TLR8 plays a distinct role in the anti-viral immune response.

Notably, these nucleotide-sensing TLRs are localized to intracellular compartments. Human TLR3 localizes to the early endosome where it recognizes exogenous dsRNA and generates signals via Toll/interleukin-1 receptor (TIR)-containing adaptor molecule-1 (TICAM-1), also named TIR domain-containing adaptor-inducing IFN-β [8,18–20]. A linker region between the transmembrane domain and the TIR domain consisting of 26 amino acids determines the subcellular localization of human TLR3 [21]. In contrast, the transmembrane domain is the main determinant for intracellular localization of mouse TLR7 and TLR9 [22,23]. The endoplasmic reticulum (ER)-resident membrane protein, UNC93B1, physically associates with TLR7 and TLR9 and delivers them to endolysosomes [24,25]. After the trafficking of TLR7 and TLR9 from the ER to the endolysosome, their ectodomains are cleaved to generate a functional receptor [26,27]. UNC93B1 also interacts with TLR3 [24], but its role in the intracellular trafficking of TLR3 remains undefined; however, the interaction of UNC93B1 with the TLR3, 7, and 9 transmembrane regions is essential for the signaling function of these TLRs [28,29]. In contrast, there is little information concerning the subcellular localization and trafficking of human TLR8.

In this study, we analyzed the subcellular localization of TLR8 in human monocytes and HeLa transfectants and demonstrated that TLR8 was localized to the early endosome and the ER but not to the late endosome or lysosome. Using a series of TLR8

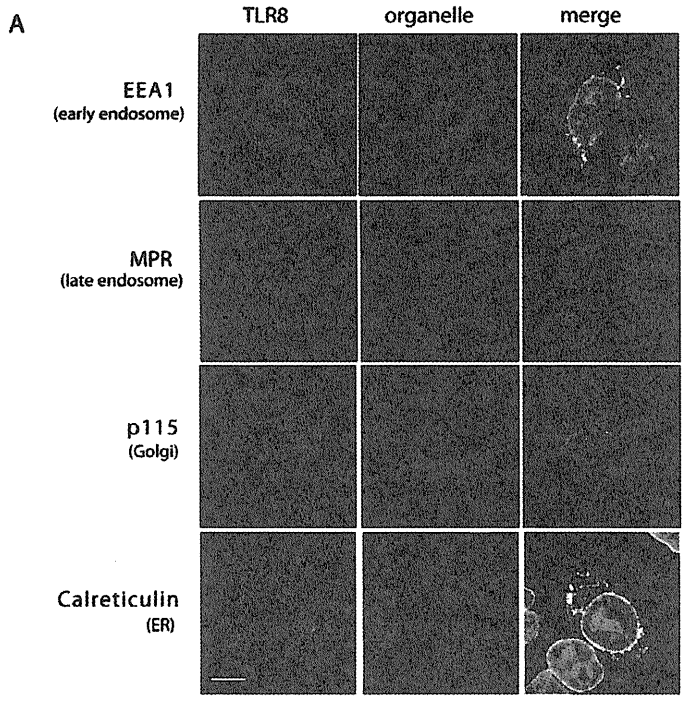
A
TLR8
organelle
merge
EEA1
(early endosome)
MPR
(late endosome)
p115
(Golgi)
Calreticulin
(ER)

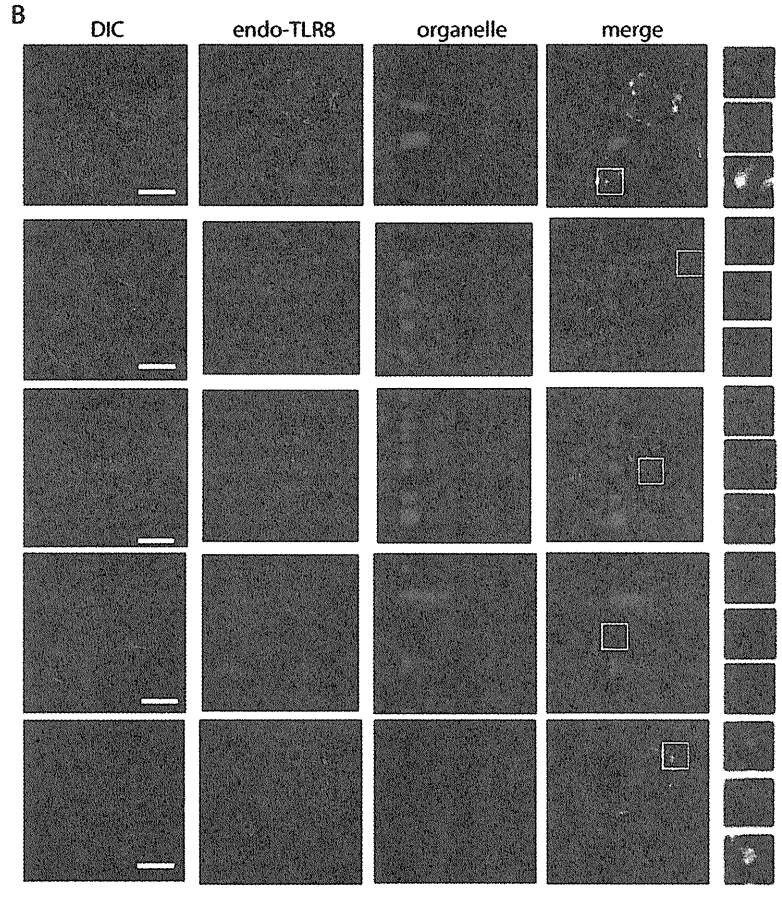
B
DIC
endo-TLR8
organelle
merge

**Figure 1. Subcellular localization of TLR8 in human monocytes and HeLa transfectants.** HeLa cells transiently expressing human TLR8 (*A*) and human monocytes (*B*) were incubated with anti-FLAG mAb (*A*) or anti-TLR8 mAb (*B*) followed by an Alexa Fluor 488-conjugated secondary Ab. Organelles were stained with an anti-EEA1 pAb, anti-MPR pAb, anti-p115 pAb, anti-calreticulin pAb, or anti-calnexin pAb followed by an Alexa Fluor 568-conjugated secondary Ab. Representative confocal images are shown. Green, TLR8; red, organelle markers; blue, nuclei stained with DAPI. Scale bar: (*A*) 10 μm; (*B*) 5 μm.
doi:10.1371/journal.pone.0028500.g001

deletion mutants, we demonstrated that both the transmembrane and the TIR domains are required for the intracellular localization of TLR8. Furthermore, we showed that UNC93B1 physically associates with TLR8 and regulates TLR8-mediated signaling.

## Results

### Human TLR8 localizes to the early endosome and the ER in human monocytes

Intracellular expression of TLR8 was first analyzed using a chimeric receptor composed of the extracellular domain of murine TLR4 fused with the transmembrane and cytoplasmic regions of murine TLR8 [22]. Subsequently, intact human TLR8 was shown to localize intracellularly in transfected cells [30]. However, the site of localization of TLR8 remained unknown. We therefore analyzed the subcellular localization of human TLR8 in HeLa cells transiently expressing FLAG-tagged human TLR8. When examined using confocal microscopy, TLR8-positive compartments colocalized with the early endosome antigen 1 (EEA1) and the ER marker calreticulin (Fig. 1A). Late endosome (MPR), lysosome (LAMP-1), and Golgi (p115) markers did not colocalize with TLR8 (Fig. 1A and data not shown). TLR8 is expressed in human monocytes and induces the cytokine production in response to a synthetic TLR8 ligand [13]; therefore, we next examined the subcellular localization of endogenous TLR8 in human monocytes. TLR8 was localized to the early endosome and the ER but not to the late endosome/lysosome or Golgi (Fig. 1B). Thus, the localization site of TLR8 differed from TLR7 and TLR9, both of which reside in the endolysosome and the ER.

### The TIR domain is required for endosomal localization of human TLR8

To determine which region is responsible for the intracellular localization and trafficking of human TLR8, we constructed tail-truncated mutants (Fig. 2A). These included a mutant lacking the TIR domain but retaining the proximal 31 amino acids (delTIR, 1–896 a.a.), one that lacked the cytoplasmic tail (delCYT, 1–866 a.a.), and a mutant lacking the transmembrane domain and the cytoplasmic tail, which anchors the receptor to the membrane via glycosylphosphatidylinositol (GPI) (GPI-TLR8, 45–843 a.a.) (Fig. 2A). When transiently expressed in HEK293FT cells, these mutant proteins were expressed with the expected molecular weight (Fig. 2B). Immunofluorescence staining of HeLa transfectants with anti-FLAG mAb showed that both delTIR and delCYT were displayed on the cell surface (Fig. 2C), while GPI-TLR8 resided only in the ER (Fig. 2C). The lack of expression of GPI-TLR8 on the cell surface was confirmed by flow cytometric analysis with an anti-FLAG mAb (Fig. S1). These results suggest that both transmembrane and the TIR domains are required for proper targeting of human TLR8 to the early endosome.

### UNC93B1 physically associates with human TLR8

The ER membrane protein UNC93B1 interacts with TLR3, TLR7, and TLR9 in the ER through the transmembrane domain, and is critical for signaling by these TLRs. Imaging analyses revealed that UNC93B1 regulates intracellular trafficking and endolysosomal targeting of TLR7 and TLR9 [25]. However, its participation in TLR8 localization and signaling remains unknown. To determine the role of UNC93B1 in TLR8 function, we constructed an additional two TLR4/8 chimeric receptors and examined physical interaction between human UNC93B1 and wild-type TLR8, TLR4/8 chimeric receptors, or tail-truncated mutants using co-immunoprecipitation analysis. Chimera TLR4ecto/8 comprised the extracellular domain of TLR4 and the transmembrane and cytoplasmic regions of TLR8, while chimera TLR4/8TIR was composed of the extracellular, transmembrane, and linker regions of TLR4 and the TIR domain of TLR8 (Fig. 3A). As shown in Figure 3B, wild-type TLR8 protein co-immunoprecipitated with UNC93B1 protein in HEK293FT cell lysates, similar to the TLR3 protein. In addition, the TLR4ecto/8 chimeric protein, but not TLR4 and TLR4/8TIR proteins, physically associated with UNC93B1, indicates that the transmembrane region of TLR8 is required for interaction with UNC93B1 (Fig. 3B). Consistent with these results, the TLR8 mutant delCYT associated with UNC93B1, while GPI-TLR8 failed to interact with UNC93B1 (Fig. 3C).

### UNC93B1 colocalizes with surface-expressed TLR8 mutants

Since delTIR and delCYT appeared on the cell surface (Fig. 2C), we next examined whether UNC93B1 translocates from the ER to the plasma membrane when these mutants were forcibly expressed in HeLa cells. Interestingly, confocal imaging analysis clearly demonstrated that endogenous UNC93B1 was colocalized with delTIR and delCYT at the plasma membrane, whereas wild-type TLR8 colocalized with UNC93B1 intracellularly (Fig. 4A).

Notably, delTIR and delCYT mutants performed as a dominant-negative against wild-type TLR8. As illustrated in Figure 4B, TLR8-mediated NF-κB activation induced with the TLR8 ligand, CL075 (a thiazoloquinolone derivative), was inhibited by the expression of either delTIR (Fig. 4B, upper graph) or delCYT (Fig. 4B, middle graph) in a dose-dependent manner. In contrast, the expression of GPI-TLR8 did not affect CL075-induced NF-κB activation mediated by wild-type TLR8 (Fig. 4B, lower graph). Thus, the delTIR and delCYT mutants appeared to interfere with the exit of wild-type TLR8 from the ER. Indeed, there was minimal overlay of wild-type TLR8 with EEA1 when co-expressed with these mutants (Fig. S2).

### UNC93B1 is essential for TLR8-mediated signaling

Next, we investigated whether UNC93B1 was involved in TLR8-mediated signaling. CL075-induced TLR8-mediated NF-κB activation was greatly increased by the co-expression of UNC93B1 (Fig. 5A). Inversely, knockdown of endogenous UNC93B1 in HEK293 cells downregulated CL075-induced TLR8-mediated NF-κB activation (Fig. 5B). Thus, UNC93B1 is indispensable for TLR8 signaling.

Given that signaling via TLRs 3, 7, and 9 was disrupted in 3d mice, which expresses a UNC93B1 missense mutant (H412R) incapable of TLR binding [29], we constructed a human UNC93B1 mutant, hUNC93B1(H412R), and examined its ability

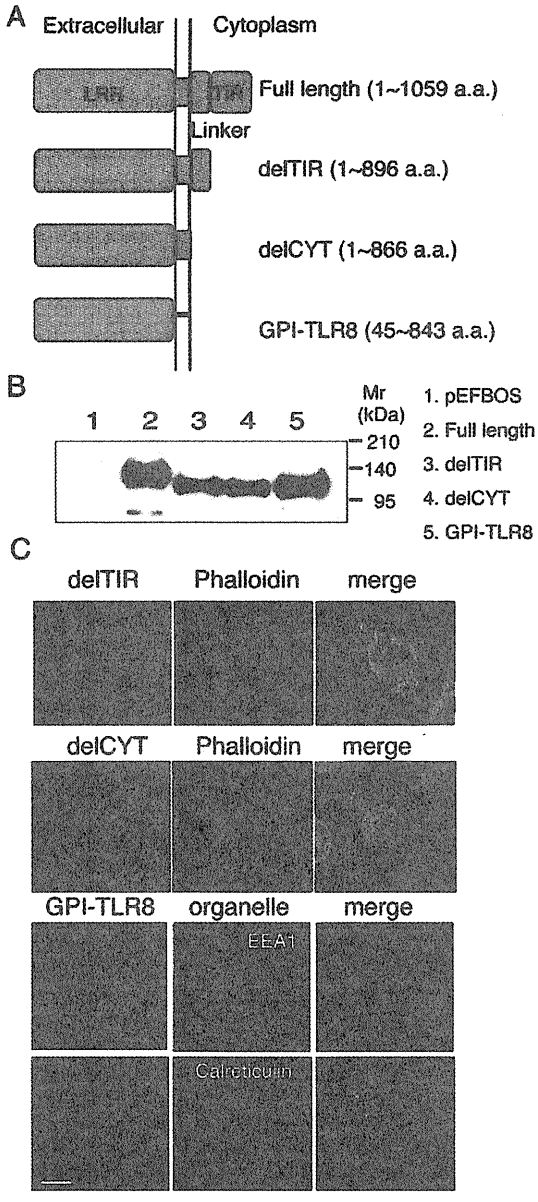


**Figure 2. Defining the TLR domain responsible for localization.** *A*, Schematic diagram of the tail-deletion constructs of hTLR8. *B*, Expression of the TLR tail-deletion constructs in HEK293FT cells. Wild-type and mutant proteins transiently expressed in HEK293FT cells were immunoprecipitated with anti-FLAG mAb, resolved using SDS-PAGE, and detected using immunoblotting with anti-FLAG mAb. Molecular weight markers are shown on the right. *C*, Immunofluorescence images of the TLR8 deletion constructs in transfected HeLa cells. The upper and middle panels show cells stained with delTIR and delCYT together with phalloidin, which labels the plasma membrane. The lower two panels show cells stained with GPI-TLR8 together with EEA1 or calreticulin. Green, TLR8 mutants; red, organelles; blue, nuclei stained with DAPI; bar, 10 μm.
doi:10.1371/journal.pone.0028500.g002

to bind to TLR8 and mediate signaling. hUNC93B1(H412R) failed to interact with human TLR8, similar to human TLR3 (Fig. 6A). Additionally, forced expression of hUNC93B1(H412R) did not augment CL075-induced TLR8-mediated NF-κB activation (Fig. 6B), suggesting that association of human UNC93B1 with TLR8 through His412 is required for TLR8-mediated signaling as was observed with mouse UNC93B1.

## Discussion

Nucleotide-sensing TLRs are divided into two groups based on their distribution profiles in DCs. In humans, TLR3 and TLR8 are expressed in myeloid DCs, while TLR7 and TLR9 are expressed in plasmacytoid DCs [6]. Although TLR8 belongs to the TLR7/8/9 subfamily, the present study demonstrated that TLR8 possesses properties distinct from those of TLR7 and TLR9. First, TLR8, like TLR3, is localized to the early endosome but not in the late endosome/lysosome, where TLR7 and TLR9 reside. Second, although TLR8 requires UNC93B1 to exit from the ER, the TIR domain determines the endosomal targeting of TLR8.

In mouse macrophages and DCs, TLR7 and TLR9 exit the ER and travel to endolysosomes where the ectodomains of both proteins are cleaved to generate functional receptors [26,27]. UNC93B1 controls intracellular trafficking of TLR7 and TLR9 [25,28]. It is obvious that UNC93B1 physically interacts with TLR3, TLR7, and TLR9 in the ER through the transmembrane domain, and is critical for signaling of these TLRs in mice [24,29]. However, prior to this study, it was unclear whether UNC93B1 was involved in TLR8-mediated signaling. We demonstrated the interaction of human UNC93B1 with human TLR8 using a co-immunoprecipitation assay and showed that the up-regulation of TLR8-mediated NF-κB activation in HEK293 cells was induced by the ectopic expression of UNC93B1 (Figs. 3 and 5). The H412R mutation within the transmembrane domain of UNC93B1 disrupted interaction between UNC93B1 and TLR8, and thus failed to increase TLR8-mediated signaling (Fig. 6). Finally, knockdown analysis revealed that UNC93B1 is indispensable for TLR8-mediated signaling (Fig. 5B).

Although UNC93B1 has been shown to deliver TLR7 and TLR9 to endolysosomes where the receptors are cleaved by proteases, this is not the case for TLR8 or TLR3. Gibbard et al. showed that the intact ectodomain of human TLR8 is necessary for dimerization of the receptor and induction of NF-κB activation in response to a synthetic ligand, CL075, in monocytes and HEK293 cells [30]. Hence, TLR8 seems to differ from TLR7 and TLR9 in its mode of ligand recognition. Interestingly, confocal analysis of TLR8 tail-truncated mutants demonstrated that endogenous UNC93B1 moved from the ER to the plasma membrane with the TLR8 mutants. In wild-type TLR8, the TIR domain controls the targeting of TLR8 to the early endosome, although UNC93B1 is required for TLR8 exit from the ER.

The nucleotide-sensing TLRs use different regulatory elements for intracellular localization. In the case of mouse TLR7 and TLR9, the transmembrane domain determines the intracellular localization of the receptor. However, Leifer et al. reported that the cytoplasmic tail of human TLR9 controls intracellular localization [31]. A 14-amino acid region in the hTLR9-TIR domain targets the Tac (human CD25)-TLR9 chimeric receptor to early endosomes. Additionally, a recent report demonstrated that bovine TLR8 localized to the ER, and that multiple regions, including ectodomain, transmembrane, linker, and TIR regions of bovine TLR8, are involved in determining the intracellular localization [32]. Thus, there may be species-specific regulatory mechanisms of intracellular localization of TLRs.

The mechanism by which TLR8 is retained in the early endosome is currently unknown. It is likely that an unidentified

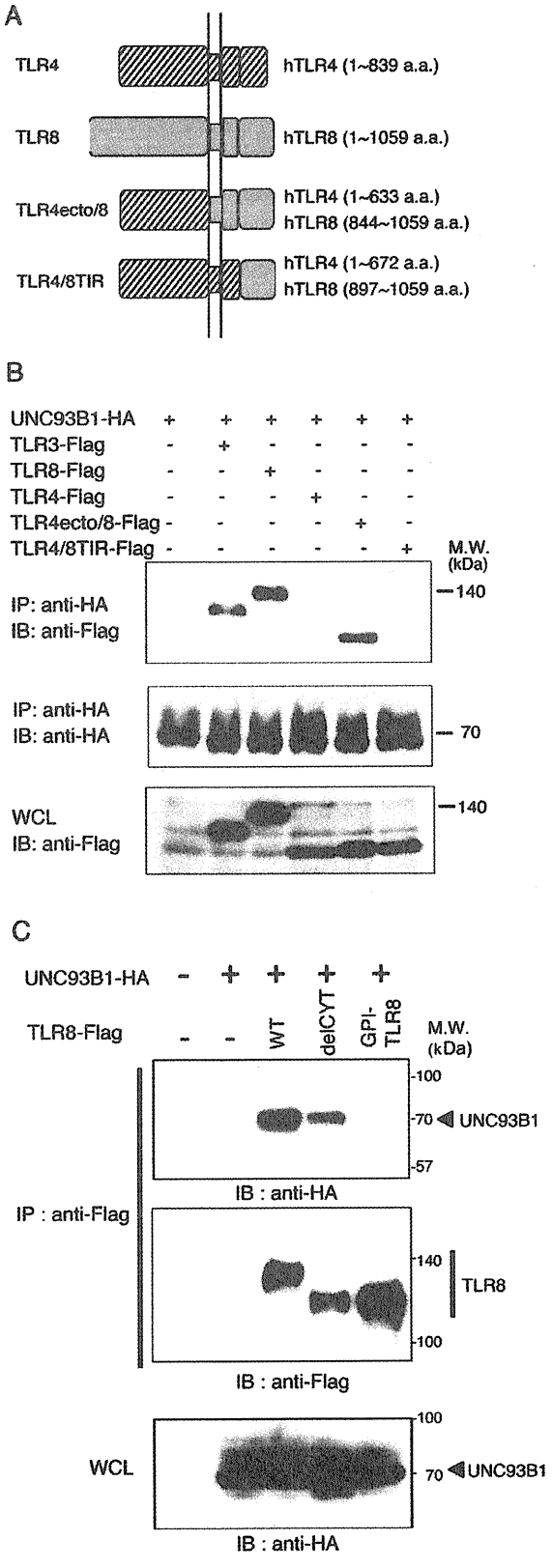


**Figure 3. UNC93B1 physically associates with TLR8 through the transmembrane domain in HEK293FT cells.** *A*, Schematic diagram of the TLR4/8 chimeric receptor constructs. *B*, *C*, HEK293FT cells were transfected with the corresponding vectors for expression of the indicated proteins. Twenty-four hours after transfection, cells were lysed in lysis buffer. The lysates were immunoprecipitated (IP) with anti-HA pAb (*B*) or anti-FLAG pAb (*C*), resolved using SDS-PAGE, and detected using immunoblotting (IB) with anti-FLAG M2 mAb or anti-HA mAb. Whole cell lysates (WCL) were subjected to immunoblotting with anti-FLAG mAb (*B*) or anti-HA mAb (*C*) to detect protein expression. Molecular weight markers are shown on the right.
doi:10.1371/journal.pone.0028500.g003

molecule interacts with the TIR domain of TLR8 and facilitates its trafficking to the early endosomes. As the BB loop in the TLR-TIR domain is critical for interaction with adaptor proteins, another region of the TLR8-TIR domain may participate in the association with the protein(s) regulating the receptor trafficking and intracellular localization of TLR8.

In humans, TLR7 and TLR8 recognize sequence-specific ssRNA and imidazoquinoline compounds in distinct cells and organelles, resulting in the induction of different immune responses via the same adaptor protein, MyD88. TLR7 ligands induce IFN-α production by plasmacytoid DCs, while TLR8 ligands induce proinflammatory cytokine production (e.g., TNF-α and IL-6) by myeloid DCs and monocytes [13]. This implies that TLR7 and TLR8 play distinct roles in the anti-viral immune response. Myeloid DCs express the viral RNA sensors, TLR3 and TLR8, on the endosomal membrane where they recognize virus-derived dsRNA and ssRNA, respectively. Activation of TLR3 by dsRNA results in the production of T helper 1 cytokines, such as IFN-α/β and interleukin (IL)-12p70, as well as DC maturation leading to the activation of cytotoxic T lymphocytes and natural killer (NK) cells [33]. TLR3 activation also induces TICAM-1-dependent gene expression in myeloid DCs, which mediates DC–NK reciprocal activation through cell–cell contact independently of type I IFN and IL-12 [34], whereas the key role of TLR8-mediated myeloid DC activation remains poorly understood. Detailed analyses of TLR8-mediated signaling in different cell types may give us new insight into the function of TLR8 in the anti-viral response.

## Materials and Methods

### Cell culture and reagents

HEK293 cells were maintained in Dulbecco's Modified Eagle's medium low glucose (Invitrogen) supplemented with 10% heat-inactivated FCS (BioSource Intl., Inc.) and antibiotics. HEK293FT cells were maintained in Dulbecco's Modified Eagle's medium high glucose supplemented with 0.1 mM NEAA, 10% heat-inactivated FCS and antibiotics. HeLa cells were maintained in Eagle's MEM (Nissui, Tokyo, Japan) supplemented with 1% L-glutamine and 10% heat-inactivated FCS. Human monocytes were isolated from peripheral blood mononuclear cells obtained from healthy individuals with a magnetic cell sorting system using anti-CD14-coated microbeads (Miltenyi Biotec, Gladbach, Germany). Anti-FLAG M2 monoclonal antibody (mAb), anti-HA polyclonal Ab (pAb), 4′,6-diamidine-2′-phenylindole dihydrochloride (DAPI), TRITC-labeled anti-phalloidin Ab, and saponin were purchased from Sigma-Aldrich. In addition, the following antibodies were used in this study: Alexa Fluor-conjugated secondary antibodies (Invitrogen), anti-HA mAb (Covance), anti-early endosome antigen 1 (EEA1) pAb (Affinity Bioreagents), anti-calnexin pAb and anti-calreticulin pAb (Stressgen, Victoria, Canada), anti-p115 pAb (Calbiochem, Darmstadt, Germany),

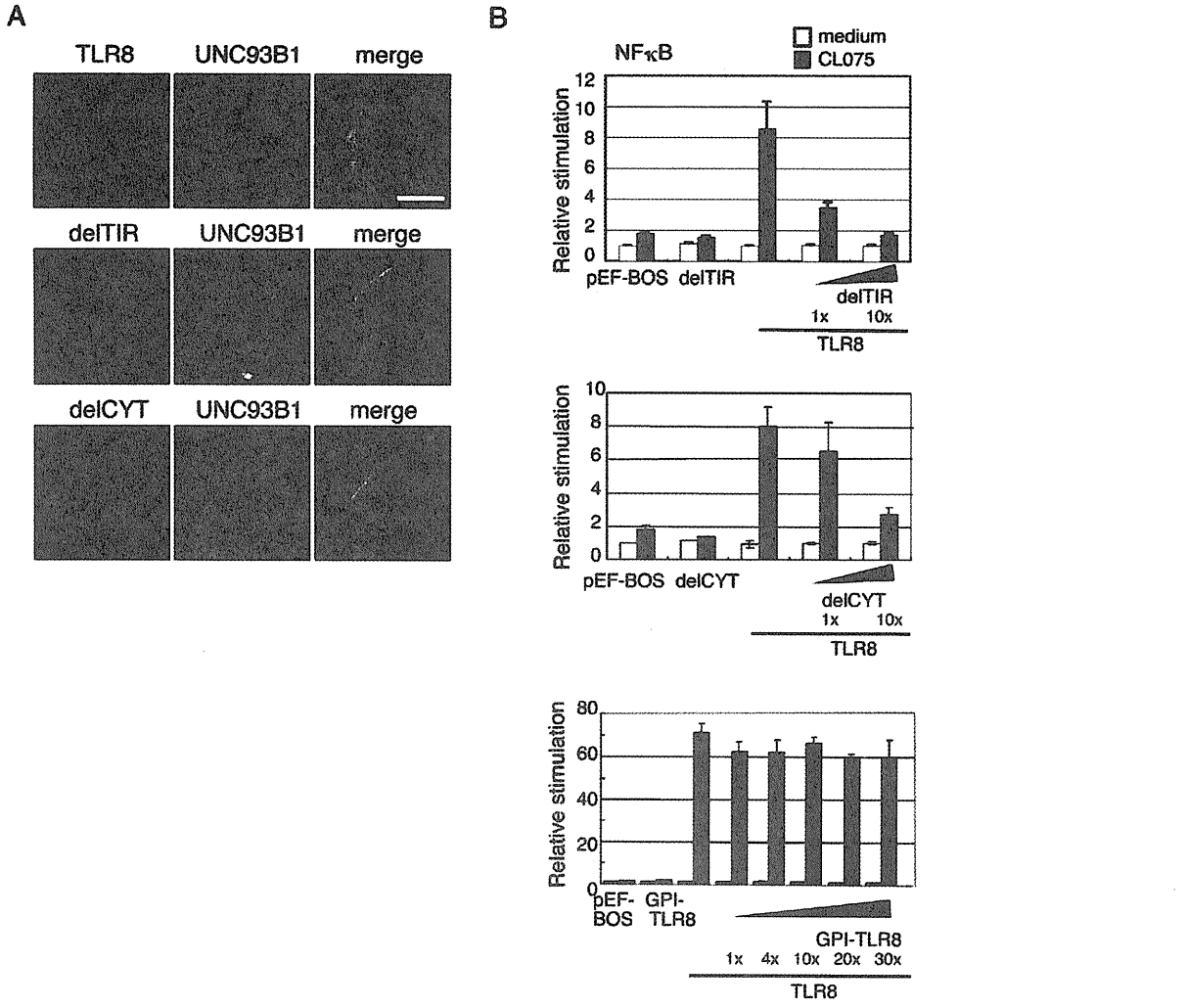


**Figure 4. UNC93B1 colocalizes with surface-expressed TLR8 mutants.** *A*, HeLa cells transiently expressing wild-type TLR8, delCYT, or delTIR were incubated with anti-FLAG mAb and anti-human UNC93B1 pAb followed by an Alexa Fluor 568-conjugated anti-mouse IgG and Alexa Fluor 488-conjugated anti-rabbit IgG. Representative confocal images are shown. Green, endogenous UNC93B1; red, TLR8; blue, nuclei stained with DAPI. Scale bar:10 μm. *B*, Surface-expressed TLR8 mutant proteins inhibited CL075-induced TLR8-mediated NF-κB activation. Luciferase activity of HEK293 cells transfected with the ELAM-promoter-luciferase reporter and expression plasmid for wild-type TLR8 together with increasing amounts of plasmid expressing delTIR (upper graph), delCYT (middle graph), or GPI-TLR8 (lower graph). Twenty-four hours after transfection, the cells were stimulated with 2.5 μg/mL of CL075 or left untreated. After 24 hours, the luciferase reporter activities were measured and expressed as the fold induction relative to the activity of unstimulated cells. Representative data from a minimum of three separate experiments are shown (mean and s.d. of triplicate assays).
doi:10.1371/journal.pone.0028500.g004

anti-LAMP-1 mAb (Biolegend), anti-MPR pAb (Abcam, Cambridge, UK), anti-human TLR8 mAb (Dendritics, LYON, France) and anti-human UNC93B1 pAb (ProSci Inc., Poway, CA). Lysotracker was from Invitrogen. CL075 was from InvivoGen.

## Plasmids

Complementary DNAs for human TLR3 and TLR8 were cloned in our laboratory by RT-PCR from the mRNA of monocyte-derived immature DCs and were ligated into the cloning site of the expression vector, pEF-BOS, which was provided by Dr. S. Nagata (Kyoto University). The FLAG-tag or HA-tag was inserted into the C-terminal of pEF-BOS expression vectors for hTLR3 or hTLR8. The truncated TLR8 mutants, delTIR (1-896 a.a.) and delCYT (1-866 a.a.) were generated by PCR with Pfu Turbo DNA polymerase (STRATAGENE) using specific primers (forward primer; 5′-GACTACAAAGACGATGACGACAAGTAAGCG-3′, reverse primer for delTIR; 5′-GAAAGTTTGCGATGTGGAAAGAGACCTGTA-3′, reverse primer for delCYT; 5′-AGCCAGGGCAGCCAACATAACCATGGTGGT-3′) as described [21]. GPI-hTLR8 was constructed in the pEF-BOS expression vector by ligation of PCR products corresponding to the TLR8 ectodomain (45-843 a.a.) sequentially attached with the preprotrypsin signal sequence, HAT, and Flag at the N-terminus, and the GPI-attachment sequence from CD55 at

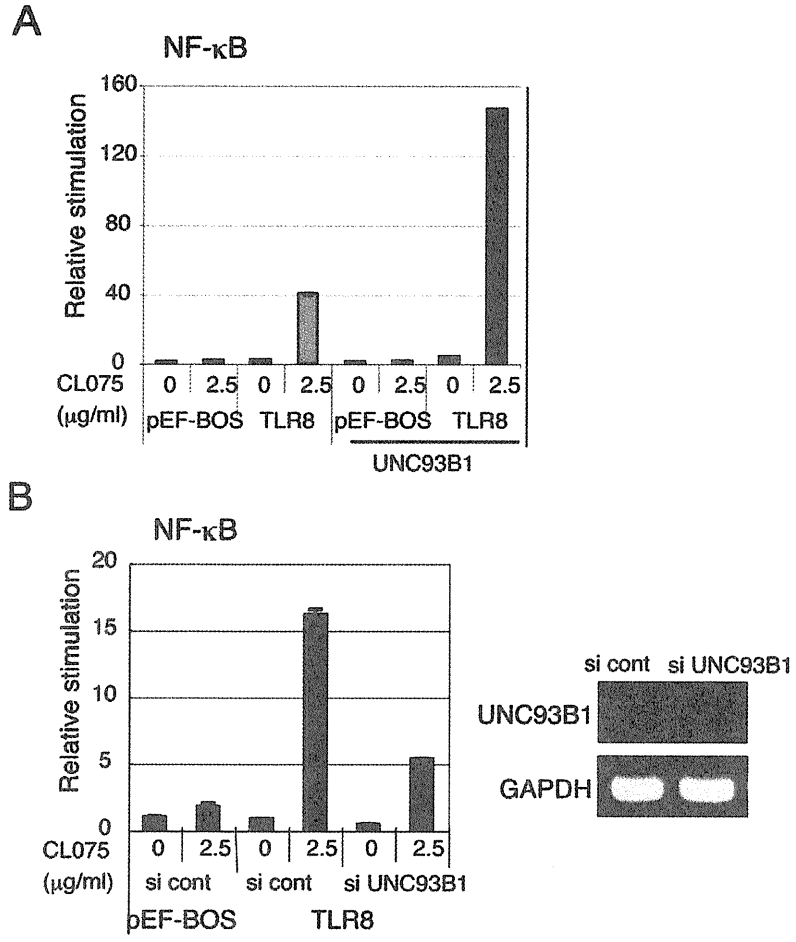


**Figure 5. UNC93B1 is indispensable for TLR8-mediated signaling.** *A*, Upregulation of TLR8-mediated NF-κB activation by co-expression with UNC93B. HEK293 cells were transfected with the indicated plasmid together with the ELAM reporter plasmid. Twenty-four hours after transfection, the cells were stimulated with CL075 or left untreated. After 6 hours, the luciferase reporter activities were measured and expressed as the fold induction relative to the activity of unstimulated cells. Representative data from three separate experiments are shown. *B*, TLR8-mediated NF-κB activation is downregulated by knockdown of UNC93B1. UNC93B1 siRNA or negative control siRNA was transfected into HEK293 cells together with the reporter plasmids and TLR8 expression plasmid. Forty-eight hours after transfection, cells were stimulated with CL075 for 6 hours and the luciferase reporter activities were measured. Data are representative of three independent experiments (mean and s.d. of triplicate assays). The expression of endogenous UNC93B1 and GAPDH mRNAs were examined using RT-PCR 48 hours after siRNA transfection (right panels).
doi:10.1371/journal.pone.0028500.g005

the C-terminus. The TLR4/TLR8 chimeric receptor, TLR4ecto/8, was constructed in the expression vector pEF-BOS by ligation of PCR products corresponding to amino acids 1-633 of human TLR4 ectodomain and amino acids 844-1059 of human TLR8. Another TLR4/TLR8 chimeric receptor, TLR4/8TIR, was constructed by the ligation of PCR products corresponding to amino acids 1-672 of human TLR4 (ectodomain, TM, and linker region) and amino acids 897-1059 of the human TLR8 TIR domain. Both constructs were FLAG tagged at the C-terminus. A plasmid for human UNC93B1 (pMD2/UNC93B1) and the expression plasmid for TLR4 (pEF-BOS/TLR4) were provided by Dr. K. Miyake (The University of Tokyo). The HA-tag was inserted into the C-terminal of the pEF-BOS expression vector for human UNC93B1. The human UNC93B1 mutant, hUNC93B1(H412R), in which the arginine residue at position 412 was substituted for a histidine residue, was made by site-directed mutagenesis.

## Confocal microscopy

HeLa cells ($1.0\times10^5$ cells/well) were plated onto micro cover glasses (Matsunami, Tokyo, Japan) in a 24-well plate. The following day, cells were transfected with the indicated plasmids using Fugene HD (Roche Diagnostics) or Lipofectamine 2000 (Invitrogen). Twenty-four hours after transfection, cells were fixed with 3% formalin for 30 min and permeabilized with PBS containing 0.5% saponin and 1% BSA for 30 min or fixed with 4% paraformaldehyde for 30 min and permeabilized with PBS containing 0.2% Triton X-100 and 1% BSA for 15 min (for staining of endogenous UNC93B1). In the case of monocytes, cells were fixed with 4% paraformaldehyde for 15 min. For the staining of late endosome, cells were permeabilized with PBS containing 100 μg/ml of digitonin and 1% BSA for 30 minutes. Fixed cells were blocked in PBS containing 1% BSA, and were then labeled with the indicated primary Abs (2~10 μg/ml) for 60 min at room temperature. Alexa-conjugated secondary Abs (1:400) were used

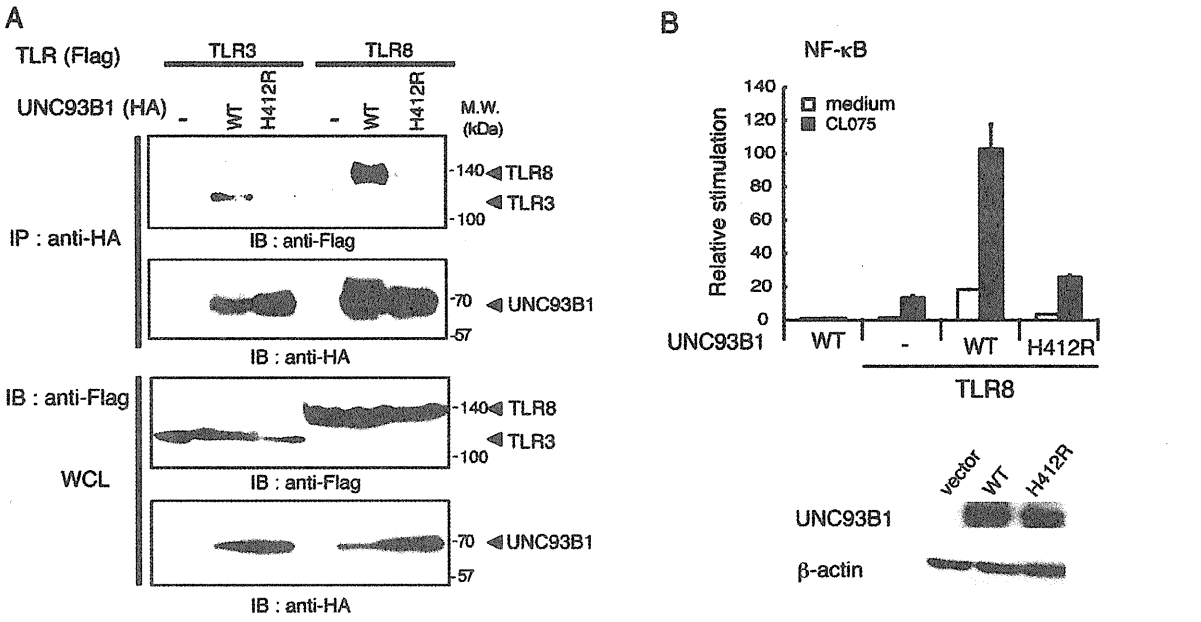


**Figure 6. His412 is essential for the interaction of UNC93B1 with TLR8 and TLR8-mediated signaling.** *A*, HEK293FT cells were transfected with the corresponding vectors for expression of the indicated proteins. The cell lysates were immunoprecipitated (IP) with anti-HA pAb, resolved by SDS-PAGE and detected by immunoblotting (IB) with anti-FLAG M2 or anti-HA mAb. Whole cell lysates (WCL) were subjected to immunoblotting with anti-FLAG or anti-HA mAb to detect protein expression. Molecular weight markers are shown on the right. *B*, HEK293 cells were transfected with the indicated plasmid together with the ELAM reporter plasmid. Cells were stimulated with CL075 or left untreated and the luciferase reporter activities were measured. Representative data from three separate experiments are shown. *Lower panels,* protein expression of wild-type and mutant UNC93B1 in HEK293 cells. β-actin blots are shown as loading controls.
doi:10.1371/journal.pone.0028500.g006

to visualize the staining of the primary Abs. After mounting with ProLong Gold with DAPI (Molecular Probes), cells were visualized at a magnification of ×63 with an LSM510 META microscope (Zeiss, Jena, Germany).

### Reporter assay

HEK293 cells ($5\times10^5$ cells/well) cultured in 24-well plates were transfected with the indicated plasmid together with the reporter plasmid and an internal control vector, phRL-TK (Promega), using FuGENE HD. The reporter plasmid containing the ELAM-1 promoter was constructed in our laboratory. Twenty-four hours after transfection, cells were stimulated with 2.5 μg/mL CL075. The cells were collected 6 hours after stimulation and then lysed. The *Firefly* and *Renilla* luciferase activities were determined using a dual-luciferase reporter assay kit (Promega). The *Firefly* luciferase activity was normalized with the *Renilla* luciferase activity and was expressed as the fold induction relative to the activity in unstimulated vector-transfected cells. All assays were performed in triplicate.

### RNAi

siRNA duplexes (UNC93B1:ID #s37730, negative control: catalog #AM4635) were obtained from Ambion-Applied Biosystems. HEK293 cells cultured in 24-well plates were transfected with 20 pmol of each siRNA together with the expression vector for hTLR8 (40 ng), ELAM reporter plasmid (60 ng), an internal control vector (1.5 ng) and empty vector (400 ng) using Lipofectamin 2000. Forty-eight hours after transfection, cells were washed once and then stimulated with 2.5 μg/ml CL075 for 6 hours. Knockdown of UNC93B1 was confirmed 48 hours after siRNA transfection by RT-PCR using specific primers (UNC93B1: forward primer 5′-GCCCATGATTTATTTCCTGAACCACTACC-3′ and reverse primer, 5′-GTGTGCTGAGTCCAGTCTTGTTCAG-3′, GAPDH: forward primer 5′-GAGTCAACGGATTTGGTCGT-3′ and reverse primer 5′- TTGATTTTGGAGGGATCTCG-3′). Experiments were repeated three times for confirmation of the results.

### Immunoprecipitation

HEK293FT cells ($2.5\times10^5$ cells/well) cultured in 12-well plates were transfected with the indicated plasmids using Lipofectamine 2000 (Invitrogen). After 24 hours, cells were washed twice with DPBS. Washed cells were lysed in 1% digitonin lysis buffer (50 mM Tris-HCl (pH 7.4), 150 mM NaCl, 5 mM EDTA, 2 mM PMSF, and a protease inhibitor cocktail) or 1% NP-40 lysis-washing buffer (50 mM Tris-HCl (pH 7.4), 150 mM NaCl, 10 mM EDTA, 1 mM PMSF, and a protease inhibitor cocktail) in Fig. 2. Lysates were clarified by centrifugation, pre-cleared with Protein G-Sepharose (GE Healthcare, Buckinghamshire, UK), and incubated with anti-FLAG mAb or anti-HA pAb. The immunoprecipitates were recovered by incubation with Protein G-Sepharose, washed three times with 0.1% digitonin washing buffer (50 mM Tris-HCl (pH 7.4), 150 mM NaCl, 5 mM EDTA, 1 mM PMSF) or 1% NP-40 lysis-washing buffer and then resuspended in denaturing buffer. Samples were analyzed by SDS-PAGE under reducing conditions followed by immunoblotting with anti-tag Abs.

## Supporting Information

**Figure S1** Flow cytometric analysis of cell surface expression of GPI-hTLR8 transiently expressed in HeLa cells. HeLa cells were

transfected with the empty vector or the expression plasmid for FLAG-tagged GPI-hTLR8 using Lipofectamine 2000 in 12-well plates. Twenty-four hours after transfection, cells were washed and incubated with anti-FLAG M2 mAb or mouse IgG1 in the presence of human IgG for 30 min at 4°C in FACS buffer (DPBS containing 0.5% BSA and 0.1% sodium azide). Cells were washed twice in FACS buffer and incubated with FITC-labeled secondary antibody (American Qualex) for 30 min at 4°C. For intracellular staining, cells were permeabilized with permeabilizing solution (BD) for 10 min at room temperature, and then stained with anti-FLAG mAb in the presence of 10% goat serum and FITC-labeled secondary Ab. Cells were analyzed using a FACS Calibur (BD). Shaded histogram: control mouse IgG 1 staining; thick line: anti-FLAG mAb staining. Inset values indicate the mean fluorescent intensities specific for the anti-FLAG mAb.
(EPS)

**Figure S2** Forced expression of TLR8 mutants affects the endosomal localization of wild-type TLR8. *A*, Confocal images show HeLa cells co-expressing HA-tagged wild-type TLR8 and FLAG-tagged TLR8 mutants. Cells were fixed and stained with anti-FLAG mAb and anti-HA pAb, followed by Alexa568-labeled goat anti-mouse Ab and Alexa488-labeled goat anti-rabbit Ab. TLR8 mutants delCYT and delTIR were anchored on plasma membrane and did not merge with wild-type TLR8. Red, TLR8 mutants; green, wild-type TLR8; blue, nuclei stained with DAPI; bar, 10 μm. *B*, Cells were transfected with FLAG-tagged wild-type TLR8 alone (upper panels), together with FLAG-tagged delCYT (middle panels) or FLAG-tagged delTIR (lower panels), and stained with anti-FLAG mAb and anti-EEA1 pAb, followed by Alexa568-labeled goat anti-mouse Ab and Alexa488-labeled goat anti-rabbit Ab. Wild-type TLR8 was expressed intracellularly and colocalized with EEA1 (upper panels). When delCYT or delTIR was expressed with wild-type TLR8, colocalization between TLR8 and EEA1 was decreased (middle and lower panels). Red, TLR8; green, early endosome marker EEA1; blue, nuclei stained with DAPI; bar, 10 μm.
(EPS)

## Acknowledgments

We are grateful to Drs. H. Oshiumi, H. Shime, T. Ebihara, A. Matsuo, H. H. Aly, H. Takaki, and J. Kasamatsu for invaluable discussions. Thanks are also due to Dr. K. Miyake (University of Tokyo, Tokyo) for providing plasmids.

## Author Contributions

Conceived and designed the experiments: HI KF TS MM. Performed the experiments: HI MT AW KI. Analyzed the data: MT TS MM. Wrote the paper: MM.

## References

1. Medzhitov R, Janeway CA, Jr. (1997) Innate immunity: the virtues of a nonclonal system of recognition. Cell 91: 295–298.
2. Akira S, Uematsu S, Takeuchi O (2006) Pathogen recognition and innate immunity. Cell 124: 783–801.
3. Kono H, Rock KL (2008) How dying cells alert the immune system to danger. Nat Rev Immunol 8: 279–289.
4. Medzhitov R, Preston-Hurlburt P, Janeway CA, Jr. (1997) A human homologue of the Drosophila Toll protein signals activation of adaptive immunity. Nature 388: 394–397.
5. Muzio M, Bosisio D, Polentarutti N, D'amico G, Stoppacciaro A, et al. (2000) Differential expression and regulation of toll-like receptors (TLR) in human leukocytes: selective expression of TLR3 in dendritic cells. J Immunol 164: 5998–6004.
6. Kadowaki M, Ho S, Antonenko S, de Waal Malefyt R, Kastelein RA, et al. (2001) Subsets of human dendritic cell precursors express different Toll-like receptors and respond to different microbial antigens. J Exp Med 194: 863–870.
7. Hornung V, Rothenfusser S, Britsch S, Krug A, Jahrsdorfer B, et al. (2002) Quantitative expression of Toll-like receptor 1-10 mRNA in cellular subsets of human peripheral blood mononuclear cells and sensitivity to CpG oligodeoxynucleotides. J Immunol 168: 4531–4537.
8. Matsumoto M, Funami K, Tanabe M, Oshiumi H, Shingai M, et al. (2003) Subcellular localization of Toll-like receptor 3 in human dendritic cells. J Immunol 171: 3154–3162.
9. Chuang T-H, Ulevitch RJ (2000) Cloning and characterization of a sub-family of human Toll-like receptors: hTLR7, hTLR8 and hTLR9. Eur Cytokine Netw 11: 372–378.
10. Du X, Poltorak A, Wei Y, Beutler B (2000) Three novel mammalian toll-like receptors: gene structure, expression, and evolution. Eur Cytokine Netw 11: 362–371.
11. Heil F, Hemmi H, Hochrein H, Ampenberger F, Kirschning C, et al. (2004) Species-specific recognition of single-stranded RNA via toll-like receptor 7 and 8. Science 303: 1526–1529.
12. Diebold SS, Kaisho T, Hemmi H, Akira S, Sousa RC (2004) Innate antivial responses by means of TLR7-mediated recognition of single-stranded RNA. Science 303: 1529–1531.
13. Gorden KB, Gorski KS, Gibson SJ, Kedl RM, Kieper WC, et al. (2005) Synthetic TLR agonists reveal functional differences between human TLR7 and TLR8. J Immunol 174: 1259–1268.
14. Jurk M, Heil F, Vollmer J, Schetter C, Krieg AM, et al. (2002) Human TLR7 or TLR8 independently confer responsiveness to the antiviral compound R-848. Nat Immunol 3: 499.
15. Ma Y, Li J, Chiu I, Wang Y, Sloane JA, et al. (2006) Toll-like receptor 8 functions as a negative regulator of neurite outgrowth and inducer of neuronal apoptosis. J Cell Biol 28: 209–215.
16. Peng G, Guo Z, Kiniwa Y, Voo KS, Peng W Fu, et al. (2005) Toll-like receptor 8-mediated reversal of CD4+ regulatory T cell function. Science 309: 1380–1384.
17. Jongbloed SL, Kassianos AJ, McDonald KJ, Clark GJ, Ju X, et al. (2010) Human CD141+ (BDCA-3+) dendritic cells (DCs) represent a unique myeloid DC subset that cross-presents necrotic cell antigens. J Exp Med 207: 1247–1260.
18. Oshiumi H, Matsumoto M, Funami K, Akazawa T, Seya T (2003) TICAM-1, an adaptor molecule that participates in Toll-like receptor 3-mediated interferon-beta induction. Nat Immunol 4: 161–167.
19. Yamamoto M, Sato S, Hemmi H, Hoshino K, Kaisho T, et al. (2003) Role of adaptor TRIF in the MyD88-independent Toll-like receptor signaling pathway. Science 301: 640–643.
20. Funami K, Sasai M, Ohba Y, Oshiumi H, Seya T, et al. (2007) Spatiotemporal mobilization of Toll/IL-1 receptor domain-containing adaptor molecule-1 in response to dsRNA. J Immunol 179: 6867–6872.
21. Funami K, Matsumoto M, Oshiumi H, Akazawa T, Yamamoto A, et al. (2004) The cytoplasmic 'linker region' in Toll-like receptor 3 controls localization and signaling. Int Immunol 16: 1143–1154.
22. Nishiya T, DeFranco AL (2004) Ligand-regulated chimeric receptor approach reveals distinctive subcellular localization and signaling properties of the Toll-like receptors. J Biol Chem 279: 19008–19017.
23. Barton GM, Kagan JC, Medzhitov R (2006) Intracellular localization of Toll-like receptor 9 prevents recognition of self DNA but facilitates access to viral DNA. Nat Immunol 7: 49–56.
24. Brinkmann MM, Spooner E, Hoebe K, Beutler B, Ploegh HL, et al. (2007) The interaction between the ER membrane protein UNC93B and TLR3, 7, and 9 is crucial for TLR signaling. J Cell Biol 177: 265–275.
25. Kim Y-M, Brinkmann MM, Paquet M-E, Ploegh HL (2008) UNC93B1 delivers nucleotide-sensing toll-like receptors to endolysosomes. Nature 452: 234–238.
26. Ewald SE, Lee BL, Lau L, Wickliffe KE, Shi G-P, et al. (2008) The ectodomain of Toll-like receptor 9 is cleaved to generate a functional receptor. Nature 456: 658–662.
27. Park B, Brinkmann MM, Spooner E, Lee CC, Kim YM, et al. (2008) Proteolytic cleavage in an endolysosomal compartment is required for activation of Toll-like receptor 9. Nat Immunol 9: 1407–141.
28. Fukui R, Saitoh S, Matsumoto F, Kozuka-Hara H, Oyama M, et al. (2009) Unc93B1 biases Toll-like receptor responses to nucleic acid in dendritic cells toward DNA- but against RNA-sensing. J Exp Med 206: 1339–1350.
29. Tabeta K, Hoebe K, Janssen EM, Du X, Georgel P, et al. (2006) The Unc93B1 mutation 3d disrupts exogeneous antigen presentation and signaling via Toll-like receptors 3, 7 and 9. Nat Immunol 7: 146–164.
30. Gibbard RJ, Morley, PJ, Gay NJ (2006) Conserved features in the extracellular domain of human Toll-like receptor 8 are essential for pH-dependent signaling. J Biol Chem 281: 27503–27511.
31. Leifer CA, Brooks JC, Hoelzer K, Lopez J, Kennedy MN, et al. (2006) Cytoplasmic Targeting motifs control localization of Toll-like receptor 9. J Biol Chem 281: 35585–35592.
32. Zhua J, van Drunen Littel-van den Hurka S, Brownliea R, Babiuka LA, Pottera A, et al. (2009) Multiple molecular regions confer intracellular localization of bovine Toll-like receptor 8. Molec Immunol 46: 884–892.

33. Matsumoto M, Seya T (2008) TLR3: Interferon induction by double-stranded RNA including poly(I:C). Adv Drug Del Rev 60: 805–812.

34. Ebihara T, Azuma M, Oshiumi H, Kasamatsu J, Iwabuchi K, et al. (2010) Identification of a polyI:C-inducible membrane protein that participates in dendritic cell-mediated natural killer cell activation. J Exp Med 207: 2675–2687.

# Herpes simplex encephalitis in children with autosomal recessive and dominant TRIF deficiency

Vanessa Sancho-Shimizu,[1,2] Rebeca Pérez de Diego,[1,2] Lazaro Lorenzo,[1,2] Rabih Halwani,[3] Abdullah Alangari,[3] Elisabeth Israelsson,[4] Sylvie Fabrega,[5] Annabelle Cardon,[1,2] Jerome Maluenda,[1,2] Megumi Tatematsu,[6] Farhad Mahvelati,[7] Melina Herman,[8] Michael Ciancanelli,[8] Yiqi Guo,[8] Zobaida AlSum,[3] Nouf Alkhamis,[3] Abdulkarim S. Al-Makadma,[9] Ata Ghadiri,[10,11] Soraya Boucherit,[1,2] Sabine Plancoulaine,[1,2] Capucine Picard,[1,2,12,13] Flore Rozenberg,[14] Marc Tardieu,[15] Pierre Lebon,[14] Emmanuelle Jouanguy,[1,2,13] Nima Rezaei,[16,17] Tsukasa Seya,[6] Misako Matsumoto,[6] Damien Chaussabel,[4] Anne Puel,[1,2] Shen-Ying Zhang,[1,8] Laurent Abel,[1,2,8] Saleh Al-Muhsen,[3] and Jean-Laurent Casanova[1,2,3,8,12]

[1]Laboratory of Human Genetics of Infectious Diseases, Necker Branch, Institut National de la Santé et de la Recherche Médicale, Necker Medical School, Paris, France. [2]University Paris Descartes, Paris, France. [3]Prince Naif Center for Immunology Research, Department of Pediatrics, College of Medicine, King Saud University, Riyadh, Saudi Arabia. [4]Benaroya Research Institute at Virginia Mason, Seattle, Washington, USA. [5]Viral Vector and Gene Transfer Platform, University Paris Descartes, Institut Fédératif de Recherche Necker Enfants Malades, Paris, France. [6]Department of Microbiology and Immunology, Hokkaido University Graduate School of Medicine, Sapporo, Japan. [7]Child Neurology Department, Mofid Children Hospital, Shahid Beheshti University of Medical Sciences, Tehran, Iran. [8]Laboratory of Human Genetics of Infectious Diseases, Rockefeller Branch, The Rockefeller University, New York, New York, USA. [9]King Fahd Medical City, Riyadh, Saudi Arabia. [10]Department of AIDS and Hepatitis, Pasteur Institute, Tehran, Iran. [11]Department of Immunology, Faculty of Medicine, Ahvaz Jundishapur University of Medical Sciences, Ahvaz, Iran. [12]Pediatric Hematology-Immunology Unit and [13]Study Center of Primary Immunodeficiencies, Necker Hospital, Paris, France. [14]Virology, Cochin Hospital, University Paris Descartes, Paris, France. [15]Pediatric Neurology, Bicêtre Hospital, University Paris Sud, Kremlin-Bicêtre, France. [16]Research Center for Immunodeficiencies, Pediatrics Center of Excellence, Children's Medical Center, and [17]Molecular Immunology Research Center and Department of Immunology, School of Medicine, Tehran University of Medical Sciences, Tehran, Iran.

**Herpes simplex encephalitis (HSE) is the most common sporadic viral encephalitis of childhood. Autosomal recessive (AR) UNC-93B and TLR3 deficiencies and autosomal dominant (AD) TLR3 and TRAF3 deficiencies underlie HSE in some children. We report here unrelated HSE children with AR or AD TRIF deficiency. The AR form of the disease was found to be due to a homozygous nonsense mutation that resulted in a complete absence of the TRIF protein. Both the TLR3- and the TRIF-dependent TLR4 signaling pathways were abolished. The AD form of disease was found to be due to a heterozygous missense mutation, resulting in a dysfunctional protein. In this form of the disease, the TLR3 signaling pathway was impaired, whereas the TRIF-dependent TLR4 pathway was unaffected. Both patients, however, showed reduced capacity to respond to stimulation of the DExD/H-box helicases pathway. To date, the TRIF-deficient patients with HSE described herein have suffered from no other infections. Moreover, as observed in patients with other genetic etiologies of HSE, clinical penetrance was found to be incomplete, as some HSV-1–infected TRIF-deficient relatives have not developed HSE. Our results provide what we believe to be the first description of human TRIF deficiency and a new genetic etiology for HSE. They suggest that the TRIF-dependent TLR4 and DExD/H-box helicase pathways are largely redundant in host defense. They further demonstrate the importance of TRIF for the TLR3-dependent production of antiviral IFNs in the CNS during primary infection with HSV-1 in childhood.**

## Introduction

Herpes simplex encephalitis (HSE) is a rare and potentially fatal manifestation of herpes simplex virus-1 (HSV-1) infection, with an incidence of about 1 in 250,000 individuals per year (1). With the introduction of acyclovir from the 1980s onward, HSE mortality rates, which used to be as high as 70%, have declined significantly (2, 3), although most patients, affected children in particular, continue to suffer life-long neurological sequelae (4–6). The incidence of HSE peaks between the ages of 6 months and 3 years, a period during which the vast majority of cases are a consequence of primary infection with HSV-1 (7–9). The pathogenesis of HSE, first described in 1941, remained elusive until the demonstration of an underlying role in this devastating disease, in at least some children, of autosomal recessive (AR) UNC-93B deficiency in 2006, autosomal dominant (AD) TLR3 deficiency in 2007, and, more recently, AD TNF receptor-associated factor 3 (TRAF3) and AR TLR3 deficiencies (10–13). Fibroblasts from patients with UNC-93B, TLR3, and TRAF3 deficiencies do not respond to stimulation with TLR3 agonists or infection with HSV-1 or vesicular stomatitis virus (VSV). HSE, together with other infectious diseases, was also reported in 2 children with mutations in STAT-1 and NEMO (10–15). These genetic deficiencies thus highlighted the importance of the TLR3-dependent production of IFN-α/β and IFN-λ after infection of the CNS with HSV-1 (6, 16, 17). In fibroblasts from patients with

**Authorship note:** Rebeca Pérez de Diego, Lazaro Lorenzo, Rabih Halwani, and Abdullah Alangari contributed equally to this work. Shen-Ying Zhang, Laurent Abel, and Saleh Al-Muhsen contributed equally to this work.

**Conflict of interest:** The authors have declared that no conflict of interest exists.

**Citation for this article:** *J Clin Invest.* 2011;121(12):4889–4902. doi:10.1172/JCI59259.

UNC-93B, TLR3, and TRAF3 deficiency (10–12) and in iPS-derived CNS cells (M. Lafaille, unpublished observations), impaired IFN production has been shown to result in enhanced viral replication and higher levels of cell death.

However, most cases of childhood HSE remain unexplained. We hypothesize that HSE is a genetically heterogeneous disease, involving a collection of single-gene inborn errors of immunity to HSV-1 in the CNS during the course of primary infection (18). Specifically, we hypothesize that mutations in genes controlling the TLR3 pathway may predispose children to HSE. Human TLR3-mediated immune responses are initiated by dsRNA intermediates in vivo or via their synthetic analog polyinosinic-polycytidylic acid [poly(I:C)] in vitro, leading to the induction of IFN-β via the NF-κB, IRF3, and AP-1 pathways (19). A principal candidate gene for HSE encodes the Toll/IL-1R (TIR) domain-containing adaptor inducing IFN-β (TRIF) protein, also known as TIR domain-containing adaptor molecule 1 (TICAM-1), due to its role as the sole adaptor of TLR3 (20–23). However, this molecule also serves as an adaptor for the MyD88-independent pathway downstream from TLR4 (24–26), raising the possibility that TRIF mutations may confer a distinct phenotype. A recent report has also shown TRIF to be involved in the detection of cytosolic dsRNA via the DExD/H-box helicase complex DDX1-DDX21-DHX36 (27). After TLR3 activation, TRIF is thought to act as a molecular platform for subsequent signaling events, recruiting TRAF3, TANK-binding kinase 1 (TBK1), NF-κB–activating kinase-associated protein 1, receptor-interacting protein 1 (RIP1), and IFN regulatory factor 3 (IRF3), in particular (28, 29). Mice lacking TRIF do not respond to poly(I:C), display impaired LPS-induced inflammatory cytokine production, and show increased susceptibility to mouse CMV and vaccinia virus infections (25, 26). Given the key role of TRIF in the TLR3 pathway demonstrated in mice, our previous demonstration of the role of the TLR3-IFN pathway in preventing the spread of HSV-1 to the CNS, and despite the potential involvement of human TRIF in TLR4 and helicase responses, we focused our candidate gene approach on TRIF by sequencing the *TRIF* gene in a cohort of children with HSE.

## Results

*Homozygous TRIF nonsense mutation in patient 1.* A patient (P1) born to consanguineous Saudi parents presented HSE at the age of 2 years (Figure 1A). This patient is now 3.5 years old and has had no other unusually severe infectious disease. No mutations were found in the coding regions of *UNC93B1* and *TRAF3*, consistent with the normal PBMC responses to TLR3, TLR7, TLR8, and TLR9 agonists (leukocyte responses to TLR3 agonists have been shown to be TLR3 independent) observed in this patient (11, 13) (Supplemental Figure 1, A and B; supplemental material available online with this article; doi:10.1172/JCI59259DS1). No mutations were found in the coding regions of *TLR3*. However, both genomic DNA (gDNA) and cDNA from the leukocytes and fibroblasts of P1 displayed a homozygous nonsense mutation in *TRIF* at nucleotide position 421 (c.421C>T), resulting in a premature termination codon replacing an arginine residue at amino acid position 141 (R141X) (Figure 1, B and C). P1 is the proband and the only member of this family homozygous for this mutation. There are no other reports of premature termination mutations in *TRIF*, and this mutation was found neither in the NCBI or Ensembl databases nor in the 1,234 unrelated healthy controls sequenced, including 1,050 individuals from the Centre d'Etude du Polymorphisme Humain–Human Genome Diversity (CEPH-HGD) panel and 182 Saudi Arabian controls (a total of 2,464 chromosomes). The premature termination codon occurs at position 141, resulting in no detectable protein in SV40 fibroblasts and EBV-transformed B cells (EBV-B cells) from the patient, as shown by Western blotting (Figure 1D and Supplemental Figure 2A). *TRIF* mRNA levels in fibroblasts and EBV-B cells from P1 were similar to those in controls, as shown by quantitative real-time PCR (Q-PCR) and full-length TRIF RT-PCR, suggesting that there is little or no nonsense-mediated mRNA decay (Figure 1E and Supplemental Figure 2B). These data suggest that TRIF R141X is a null allele, causing complete TRIF deficiency in P1.

*Heterozygous TRIF missense mutation in P2.* A girl (P2) of mixed European descent (French, Portuguese, and Swiss) presented HSE at the age of 21 months (Figure 2A). The patient is now 18 years old and has had no other unusually severe infectious disease. Mutations in all known HSE-causing genes were excluded, not only for the coding regions of *UNC93B1* and *TRAF3*, consistent with the normal responses to TLR3, TLR7, TLR8, and TLR9 agonists observed (Supplemental Figure 1, C and D), but also for the coding regions of *TLR3*. However, both gDNA) and cDNA from the leukocytes and fibroblasts of P2 displayed a heterozygous nucleotide substitution in *TRIF* at position 557 (c.557C>T), resulting in the substitution of a leucine for a serine residue at amino acid position 186 (S186L) (Figure 2, B and C). P2 is the proband and the only member of this family to have developed HSE. However, the mother and maternal grandfather of P2 also carry the S186L mutation and have HSV-1–specific serum antibodies. This mutation was not found in the NCBI and Ensembl databases or in the 1,050 unrelated healthy controls from the CEPH-HGD panel sequenced, including 289 Europeans (a total of 2,100 chromosomes). Serine 186 is conserved in 8 out of the 11 animal species with TRIF proteins sharing over 50% homology to the human protein (Figure 1D). Leucine has never been found in position 186 in any species, although 2 nonhuman primates and the horse carry an alanine residue at this position, whereas the mouse has a proline residue. The S186L mutation affects the N-terminal region of the protein (Figure 1C). Previous studies have shown that the N-terminal region of TRIF plays an important role, as an N-terminal deletion mutant (including S186) displayed a specific loss of IRF3 activation and IFN-β promoter induction (21, 25). *TRIF* mRNA and protein levels in the fibroblasts and EBV-B cells of P2 were found to be similar to those in controls, suggesting that the transcription and expression of the gene were not affected by this or any other undetected mutation (Figure 1, E and F, and Supplemental Figure 2, A and B). These data suggest that TRIF S186L is a rare allele and that the missense mutation may cause an AD form of TRIF deficiency, conferring a predisposition to HSE with incomplete clinical penetrance (similar to both UNC-93B and TLR3 deficiencies) (10, 11).

*Impaired cellular responses to TLR3 agonists.* Dermal fibroblasts from P1 and P2 were used to investigate the AR R141X and AD S186L *TRIF* mutations. After 24 hours of stimulation with poly(I:C), the fibroblasts of P1 and P2 displayed impaired production of IFN-β, IFN-λ1/3 (IL-29/IL-28B), and IL-6 similar to that observed in cells from UNC-93B–deficient patients and contrasting with the situation in cells from a healthy control ($P < 0.05$ for all comparisons) (Figure 3A). Cells from another TRIF heterozygote, the mother of P2, also showed impaired production of IFN-β, IFN-λ1/3, and IL-6 compared with that of a control ($P < 0.05$ for all comparisons) after

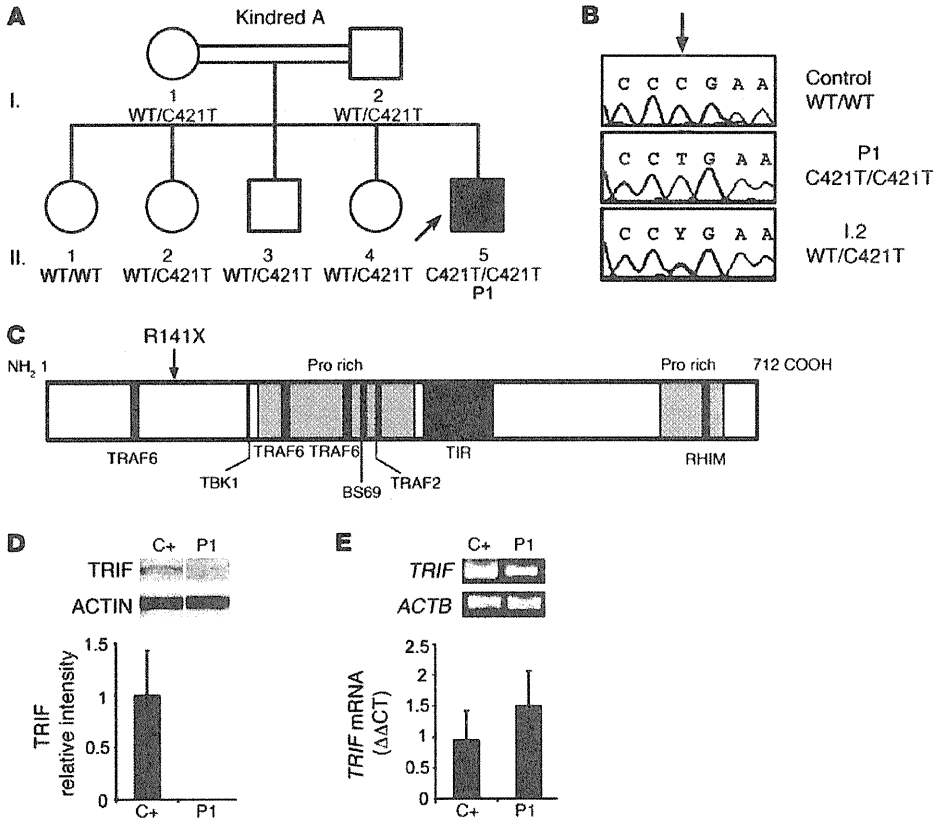


**Figure 1**

AR TRIF deficiency in P1. (**A**) Family pedigree of kindred A with allele segregation of the mutation. The HSE patient is shaded in black. Roman numerals (left margin) indicate generations. An arrow indicates the proband. (**B**) Automated sequencing profiles for the TRIF C421>T mutation in gDNA isolated from leukocytes from a healthy unrelated control; the patient, P1; and the father, I.2. The arrow indicates the position of the mutation. (**C**) A schematic representation of the TRIF protein (1–712 amino acids) indicating the amino acid position, R141X, affected by the C421>T mutation. Proline-rich domains (pro rich) are shaded in gray; functional domains are shaded in black (TRAF6 binding, TIR, RIP homotypic interacting motif [RHIM]). (**D**) TRIF protein expression by immunoblot analysis of SV40 fibroblast cell lysates from a healthy control (C+) and P1. Samples were migrated on the same blot. TRIF expression levels were quantified by densitometry results normalized with respect to ACTIN levels and expressed as relative intensity of TRIF. This is a representative blot from 3 independent experiments (mean ± SEM). (**E**) RT-PCR of full-length *TRIF* cDNA is shown with *ACTB* cDNA as an internal control. *TRIF* cDNA levels were assessed by real-time PCR in control fibroblasts (C+) and P1. Data are represented as relative fold change (ΔΔCt units), where *GUS* was used for normalization. An average of 3 independent experiments is represented (mean ± SEM).

24 hours of stimulation with various doses of poly(I:C) (Supplemental Figure 3). Consistent with the lack of IFN-β induction in P1, no IRF3 dimers were found in P1 or in cells from a patient with complete UNC-93B deficiency (negative control). In P2, IRF3 dimerization in response to poly(I:C) was impaired but not abolished. By contrast, cells from a patient with MyD88 deficiency and cells from a healthy individual (positive control) were able to form dimers as early as 1 hour after stimulation (Figure 3B). Nuclear translocation of the p65 subunit of NF-κB after poly(I:C) stimulation was also abolished in P1 cells ($P < 0.05$) and reduced in P2 cells ($P < 0.05$) compared with that in a control (Figure 3C). However, NF-κB activation in P1 and P2 cells was normal after stimulation with IL-1β and TNF-α. As expected, there was no p65 translocation upon IL-1β stimulation in MyD88-deficient cells or in NEMO-deficient cells. We then tested the responses of P1 and P2 to a specific noncommercial TLR3 agonist, polyadenylic-polyuridylic acid [poly(A:U)], poly(I:C) delivered intracellularly with lipofectamine, and the RIG-I–specific ligand, 7sk-as (30). There was no response to the TLR3 agonist poly(A:U) in P1 and P2 cells, whereas IFN-β, IFN-λ1/3, and IL-6 were induced in cells from P1 and P2 after transfection with poly(I:C) or 7sk-as (Figure 3D). Interestingly, both patients induced lower levels of IFN-β and IL-6 in response to transfected poly(I:C) compared with those of a control ($P < 0.05$ for all comparisons). Intracellular poly(I:C) is known to activate cytosolic dsRNA receptors, such as RIG-I and MDA5, which use the adaptor VISA to induce IRF3 and IFN-β (31, 32). Recently, however, TRIF was also shown to participate in cytosolic dsRNA receptors pathways (27). These findings demonstrate that the recognition of extracellular dsRNA was impaired in P1 and P2 cells, consistent with the established role of TRIF in the TLR3 pathway. The response to intracellular dsRNA in the cytosol was modestly affected in both patients, in line with recent reports of TRIF's involvement in cytosolic pathways. In addition, we carried out genome-wide transcriptional analysis of the TLR3 pathway

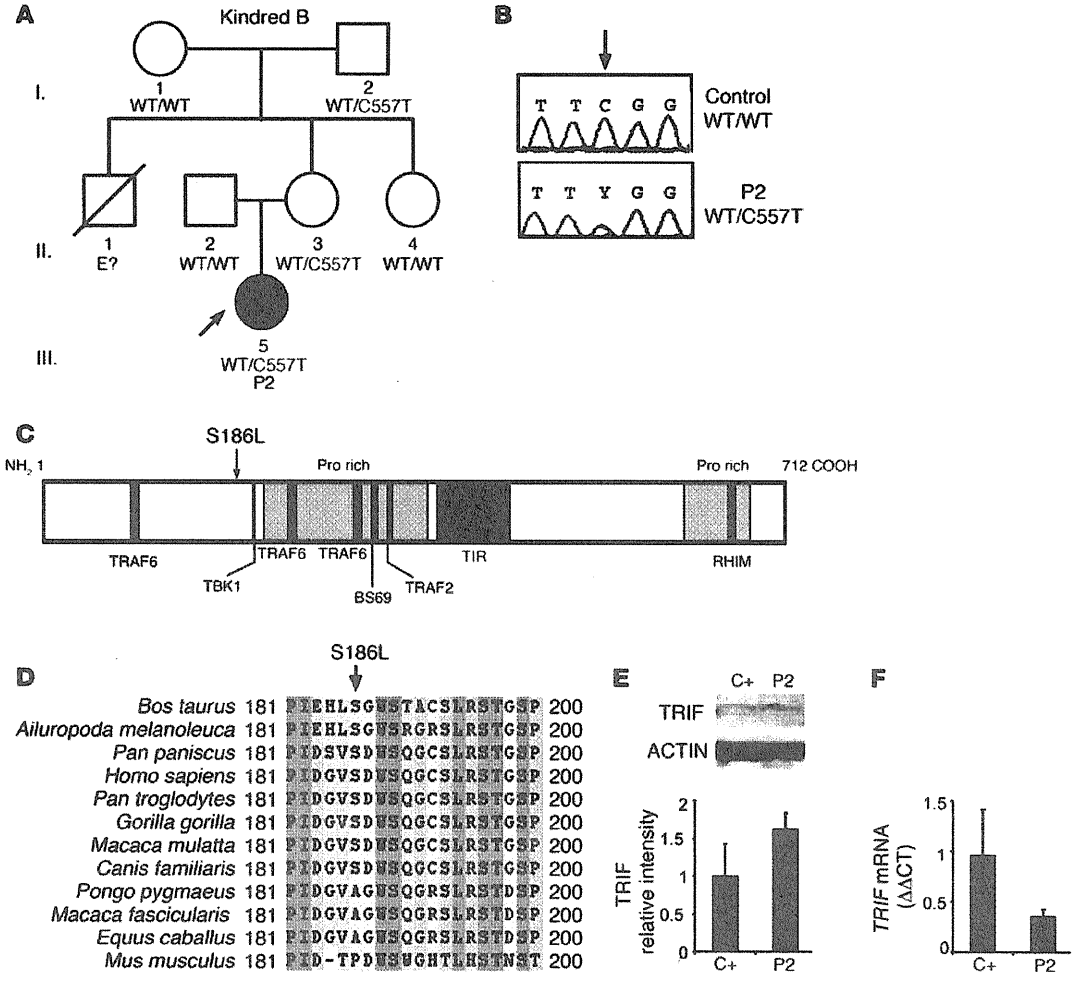


**Figure 2**

AD TRIF deficiency in P2. (**A**) Family pedigree of kindred B with allele segregation of the mutation. The HSE patient is shaded in black. Roman numerals (left margin) indicate generations. An arrow indicates the proband, and "E?" indicates an undetermined genotype. (**B**) Automated sequencing profiles for the TRIF C557>T mutation in gDNA isolated from leukocytes from a healthy unrelated control and in the patient, P2. The arrow indicates the position of the mutation. (**C**) A representation of the TRIF protein (1–712 amino acids) indicating the amino acid position, S186L, affected by the C557>T mutation. Proline-rich domains are shaded in gray; functional domains are shaded in black (TRAF6 binding, TIR, and RHIM). (**D**) Multiple alignment of TRIF amino acid sequence surrounding the mutation S186L. (**E**) TRIF protein expression by immunoblot analysis of SV40 fibroblast cell lysates from a healthy control (C+) and P2. TRIF expression levels were quantified by densitometry results normalized with respect to ACTIN levels and expressed as relative intensity of TRIF. This is a representative blot from 3 independent experiments (mean ± SEM). (**F**) *TRIF* cDNA levels were assessed by real-time PCR in control fibroblasts and P2. Data are represented as relative fold change (ΔΔCt units), where *GUS* was used for normalization. An average of 3 independent experiments is represented (mean ± SEM).

in fibroblasts of a control, P1, an AR TLR3-deficient patient, and an AR MyD88-deficient patient after 4 hours of poly(I:C) or IL-1β stimulation. In control fibroblasts, there were 506 transcripts found to be differentially regulated upon poly(I:C) (Supplemental Figure 4A). Unlike control cells or MyD88-deficient cells, P1 cells as well as the TLR3-deficient cells failed to respond to poly(I:C) (Supplemental Figure 4A), whereas their responses were normal upon IL-1β stimulation, unlike MyD88-deficient cells (Supplemental Figure 4B). Investigation of the functional pathways induced by poly(I:C) lead to the identification of genes that were induced in control cells but not in P1. These genes included IFN-regulated genes (*IFIH1*, *IFIT1*, *IFIT2*, and *IFIT3*), proinflammatory cytokines (*IFNB1*, *IL12A*, *IL15*, *IL29*, *TNFSF13B*, *TNFAIP6*, and *TNFSF10*), chemokines (*CXCL11*, *CCL3*, *CCL3L1*, *CCL3L3*, *CCL8*, *CXCL9*, *CCL5*, and *CXCR7*), and cell death/apoptosis genes (*RIPK2*, *BCL10*, *CASP7*, *BIRC2*, and *BIRC3*) (Supplemental Figure 4C). These experiments suggest that the R141X mutation results in a null allele causing AR complete TRIF deficiency, whereas the S186L *TRIF* allele is dysfunctional and causes AD dominant partial TRIF deficiency.

*Cellular response to LPS.* TRIF is known to interact with TLR4 in mice and humans (22) and has been shown to control IFN induc-